Activity indicators and the atmospheric parameters of the Kepler targets

Joanna Molenda-Żakowicz

University of Wrocław, Poland

Kepler telescope and the Kepler Input Catalog (KIC) – situation in a nutshell

- Kepler/K2: one broad-band fil
- KIC: ground-based, atmosphe
evolved stars at solar tempera
- Hot stars: atmospheric paran
et al. (2010), McNamara et al.

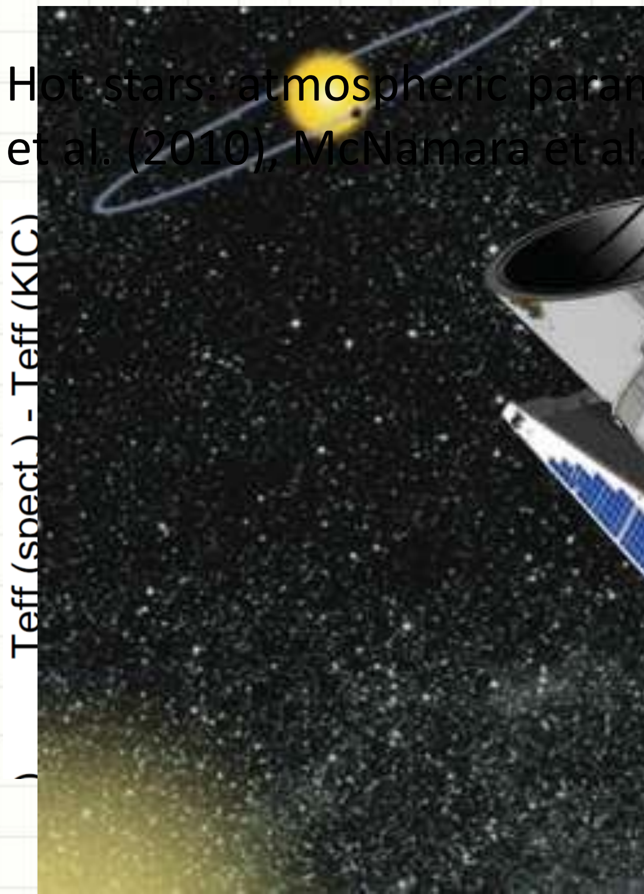

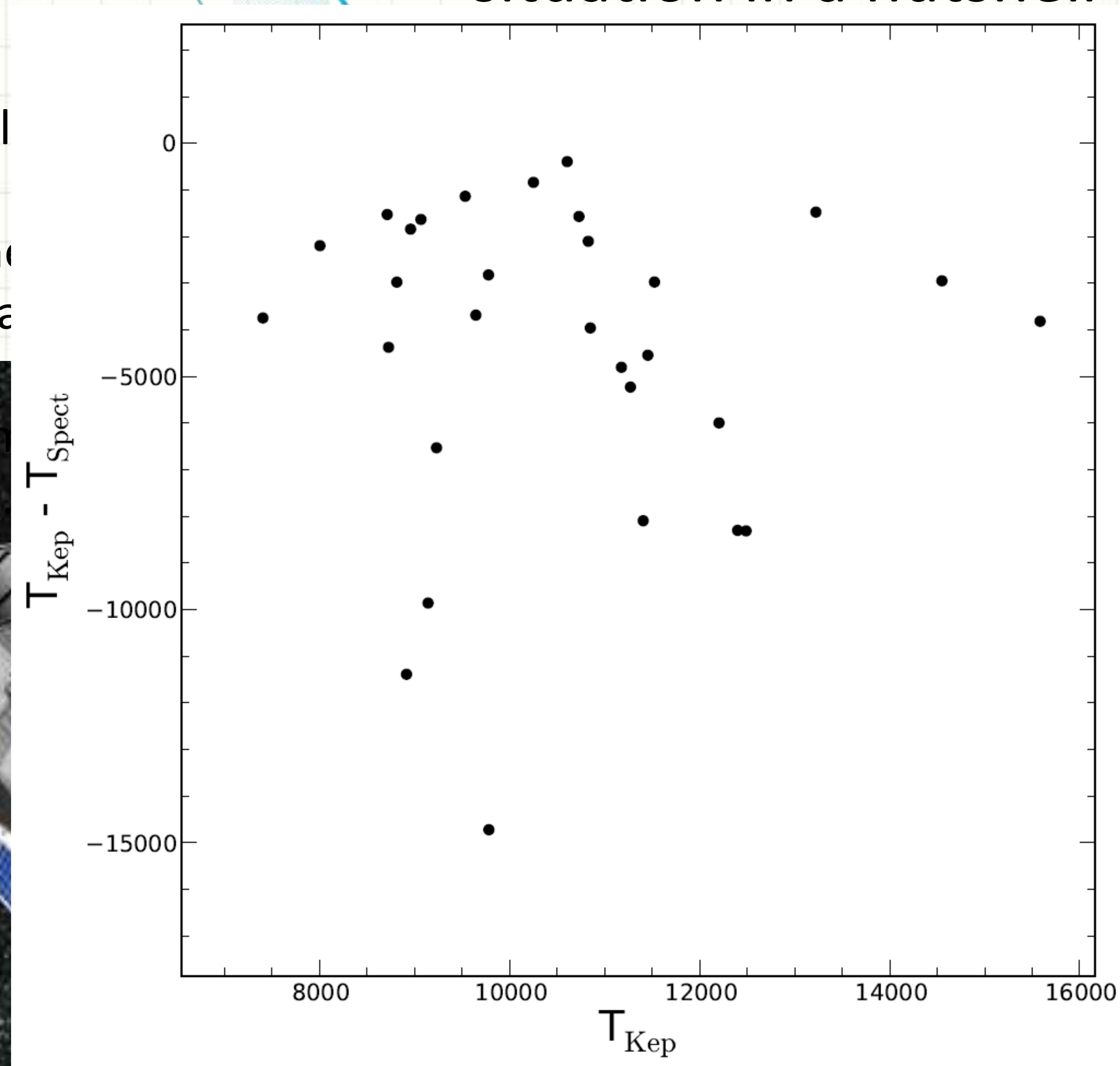

Kepler telescope and the Kepler Input Catalog (KIC) – situation in a nutshell

- Kepler/K2: one broad-band filter, very precise space photometry;
- KIC: ground-based, atmospheric parameters → distinguish main sequence from evolved stars at solar temperature;
- Hot stars: atmospheric parameters can be very imprecise (e.g. Molenda-Żakowicz et al., McNamara et al.);
- Asteroseismology: precise atmospheric parameters, especially metallicities, are crucial: KIC is not precise enough even for solar-type stars (e.g. Stello et al., Creevey et al., Metalfe et al.);
- Ground-based follow-up observations (e.g. Molenda-Żakowicz et al., Bruntt et al., Thygesen et al., and many others) → high-resolution spectroscopy of hundreds of bright stars mostly solar type; other projects dedicated to selected groups of stars;
- What about the faint stars for which often there are no data in the KIC?

The LAMOST – Kepler project

- Initiated in 2010 by J.N.Fu, P. De Cat, A. Frasca, G. Catanzaro, J. Molenda-Żakowicz, et al. with the aim of collecting low-resolution spectra of as many objects in the Kepler FoV as possible.
- Homogeneous determination of the stellar atmospheric parameters, RV, vsini, and detection of spectral peculiarities.
- Independent analyses carried out by the 'European team' (De Cat, Frasca, Catanzaro, Molenda-Żakowicz), the 'American team' (Gray and Corbally), and the 'Asian team' (Fu and Ren).

LAMOST: characteristics

- Mirror A: 5.72 m × 4.4 m
- Mirror B: 6.67 m × 6.05 m
- Field of view: 5°
- Number of fibers: 4000,
- Diameter of fibres: 320 μm (3.3 arcsec on the sky)
- Spectral range: 370-900 nm
- Spectral resolving power: R=500, 1000, 1500
- Limit magnitude: 20.5m (1.5h exposure in R=500 mode)
- Observable sky: declination range from -10° to +90°

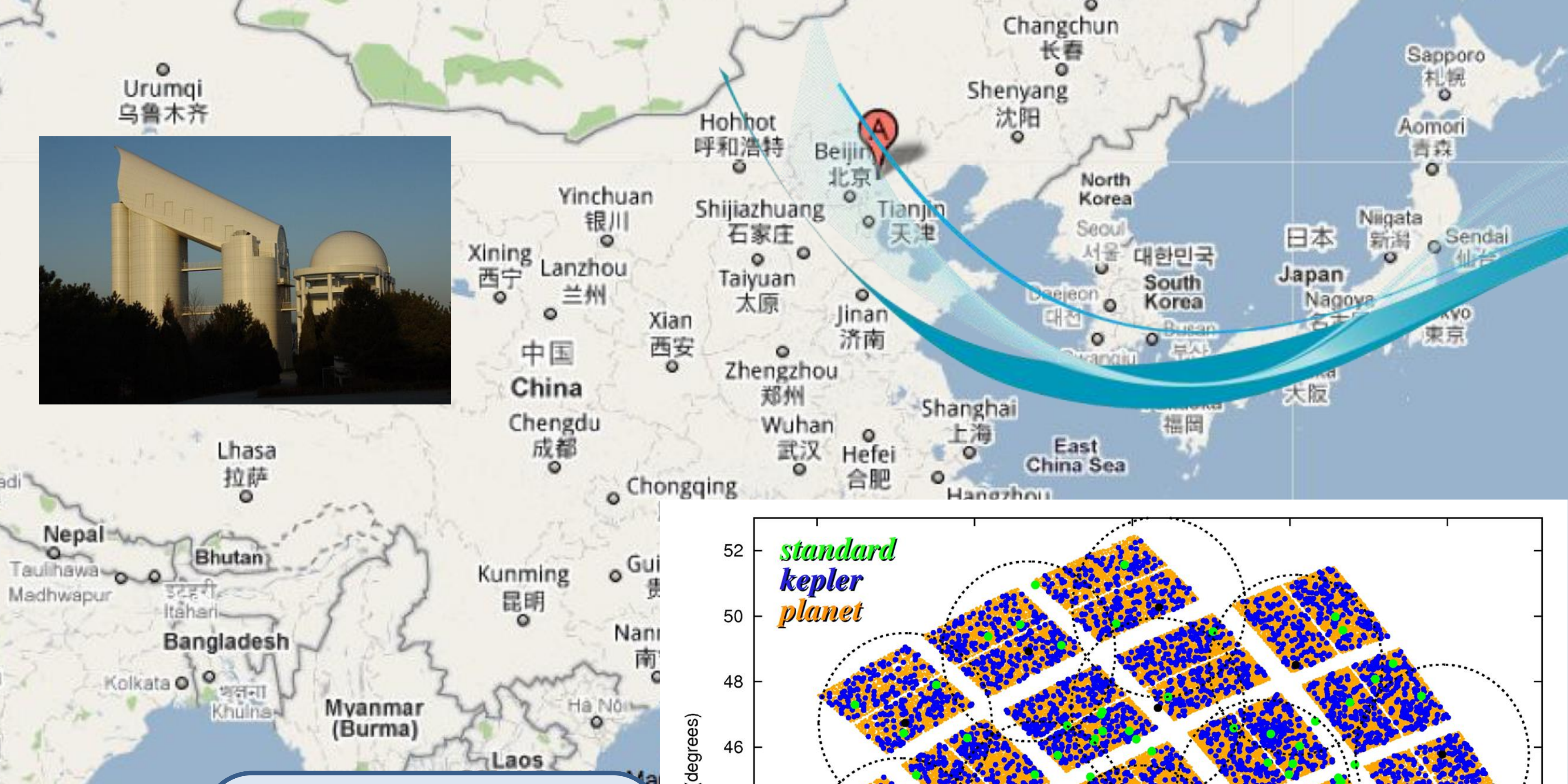

Dates:

30/05/2011
08/06/2011

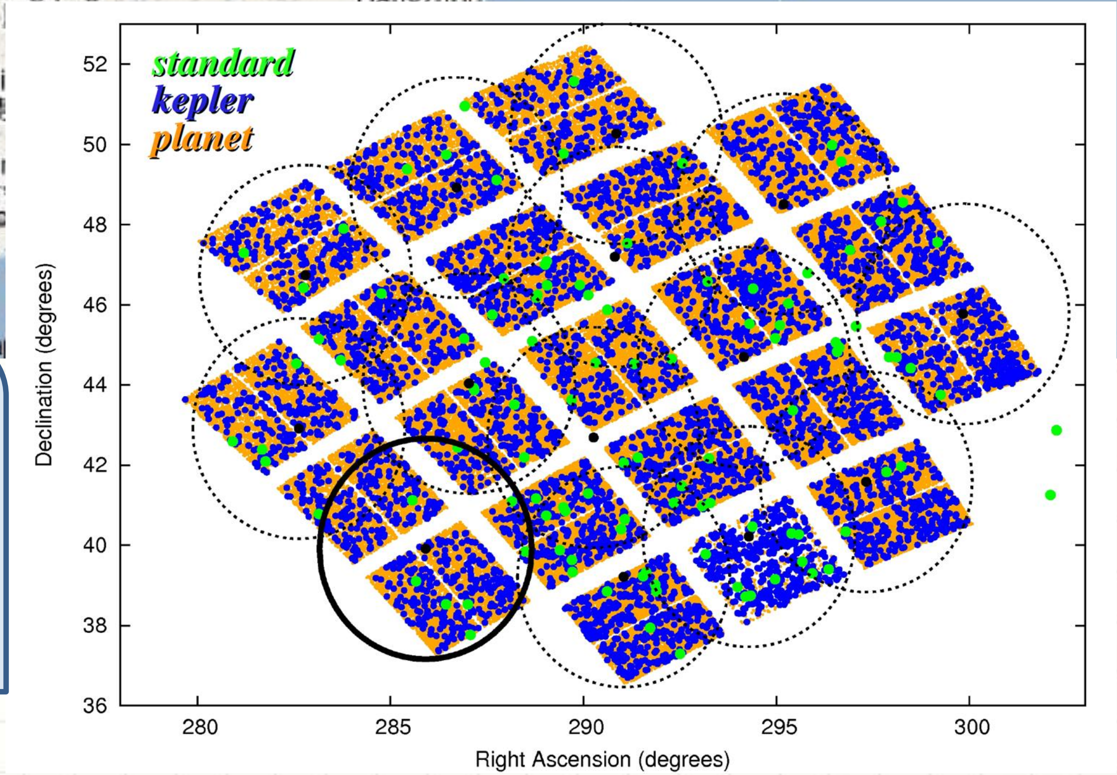

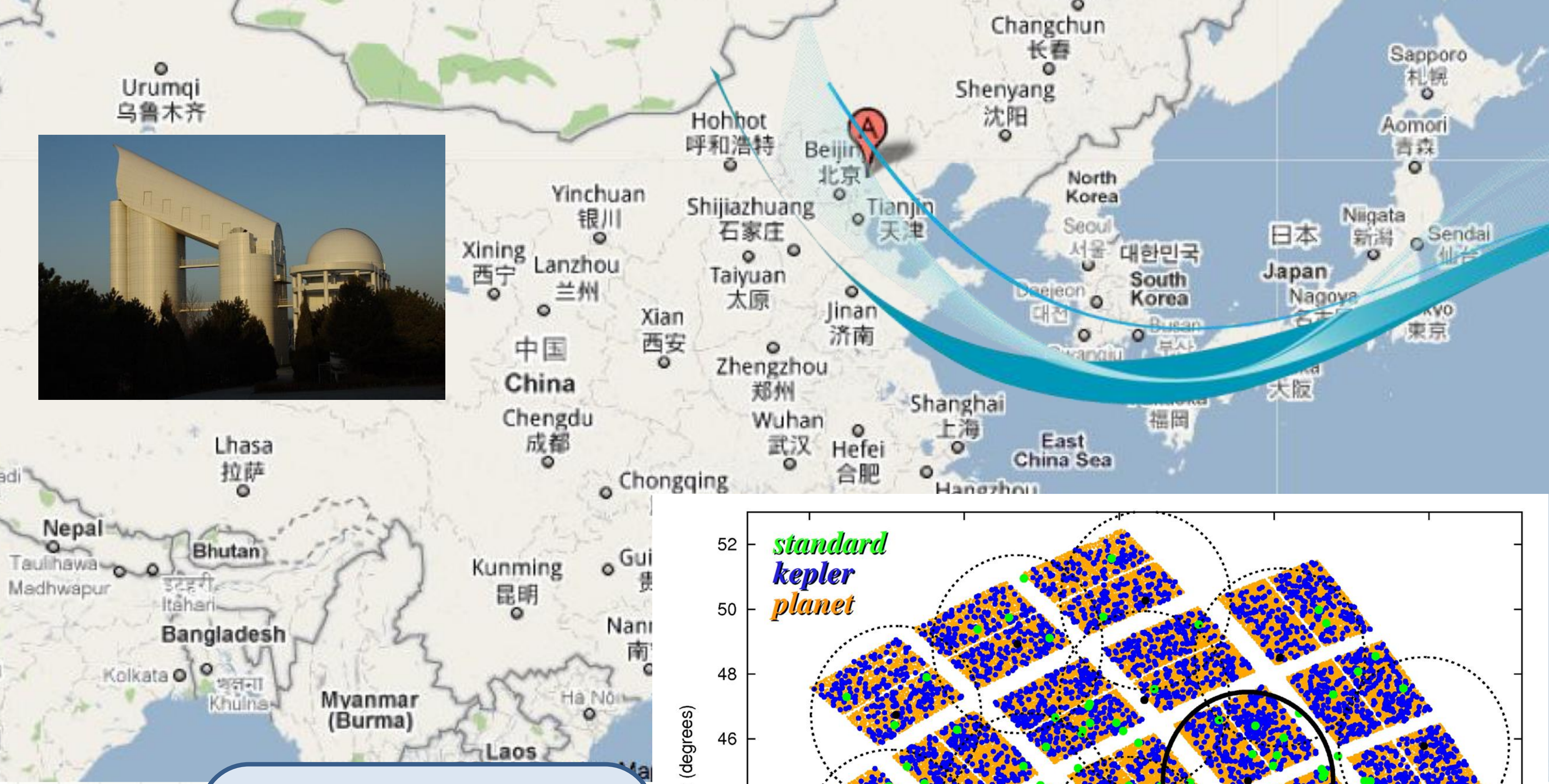

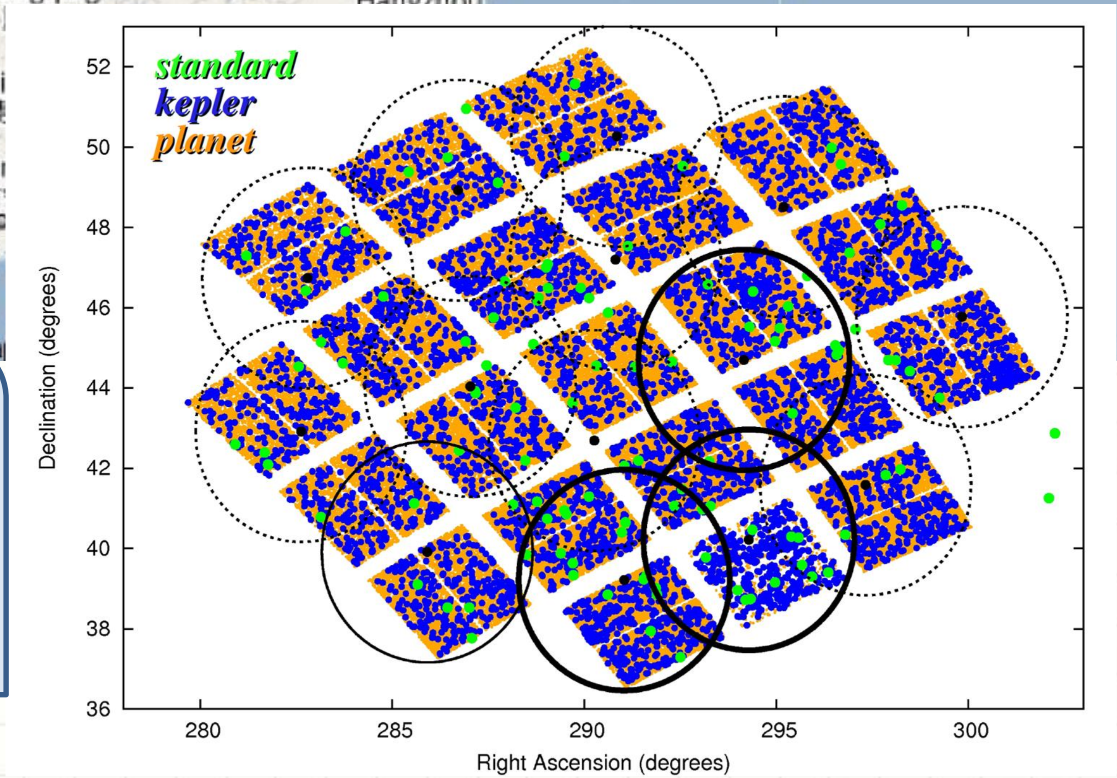

Dates:

04/06/2012
15/06/2012
17/06/2012

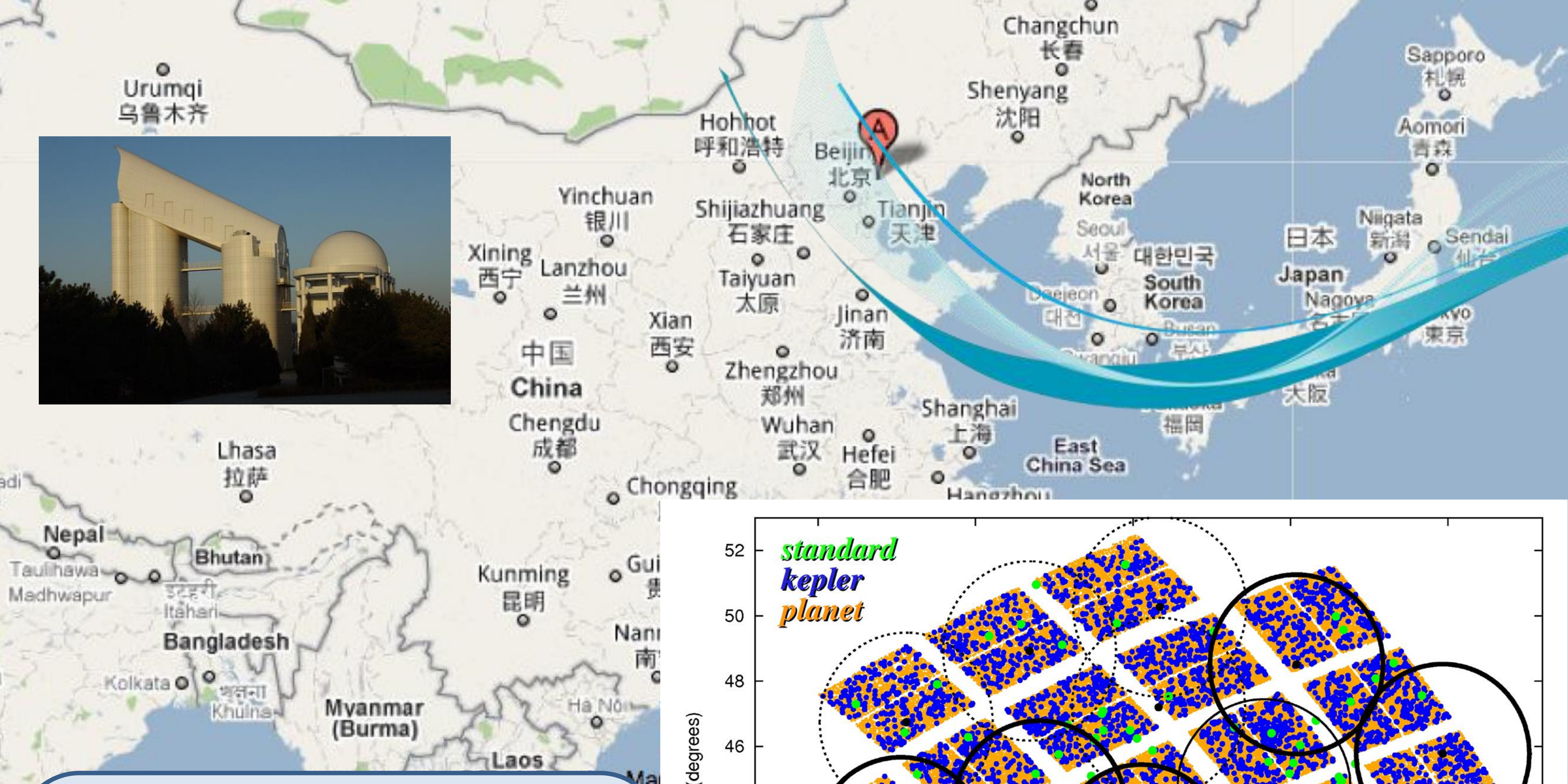

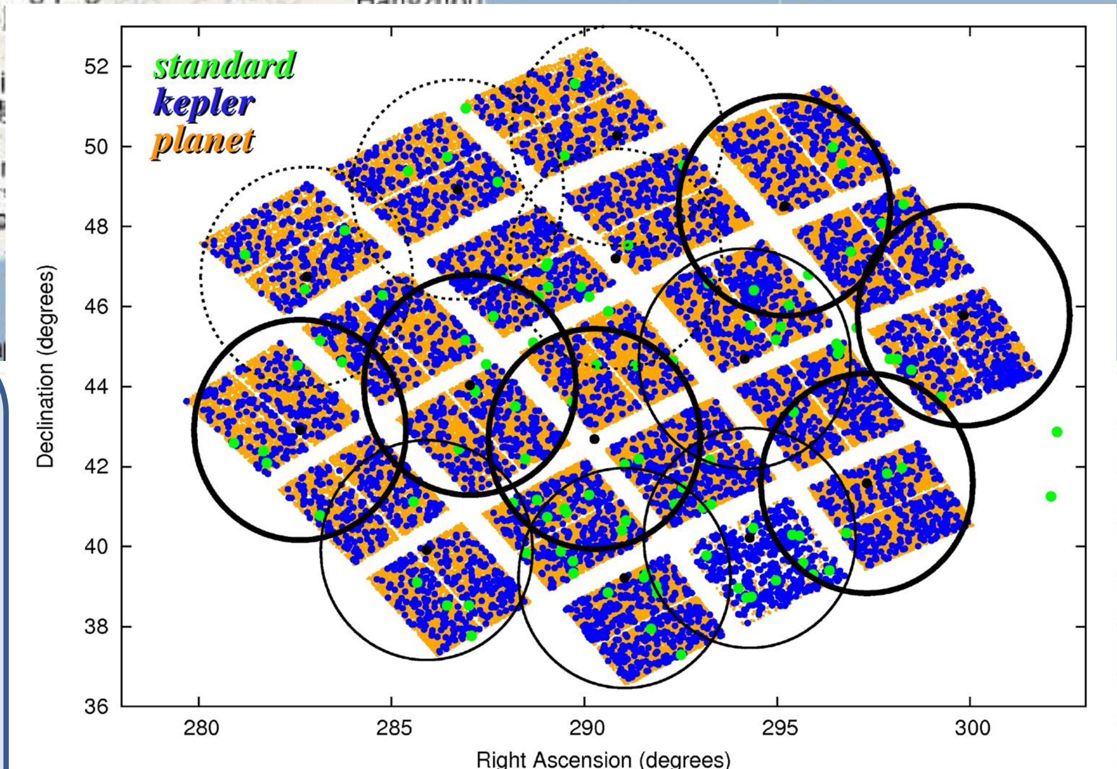

Dates:

19/05/2013 22/05/2013
14/09/2013 25/09/2013
26/09/2013 02/10/2013
04/10/2013 05/10/2013
07/10/2013 17/10/2013
25/10/2013

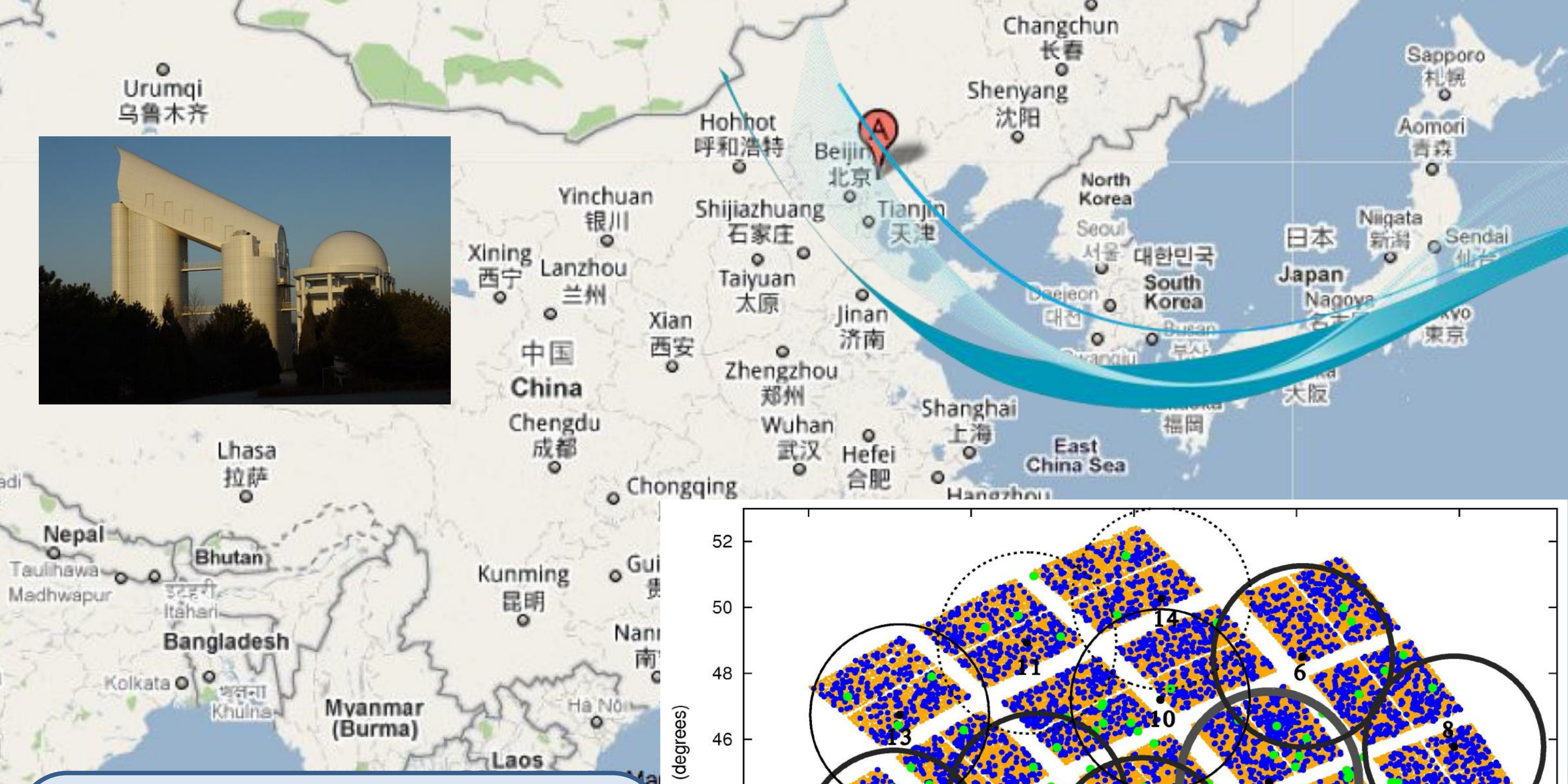

Dates:

02/05/2014 20/05/2014
22/05/2014 29/05/2014
02/06/2014

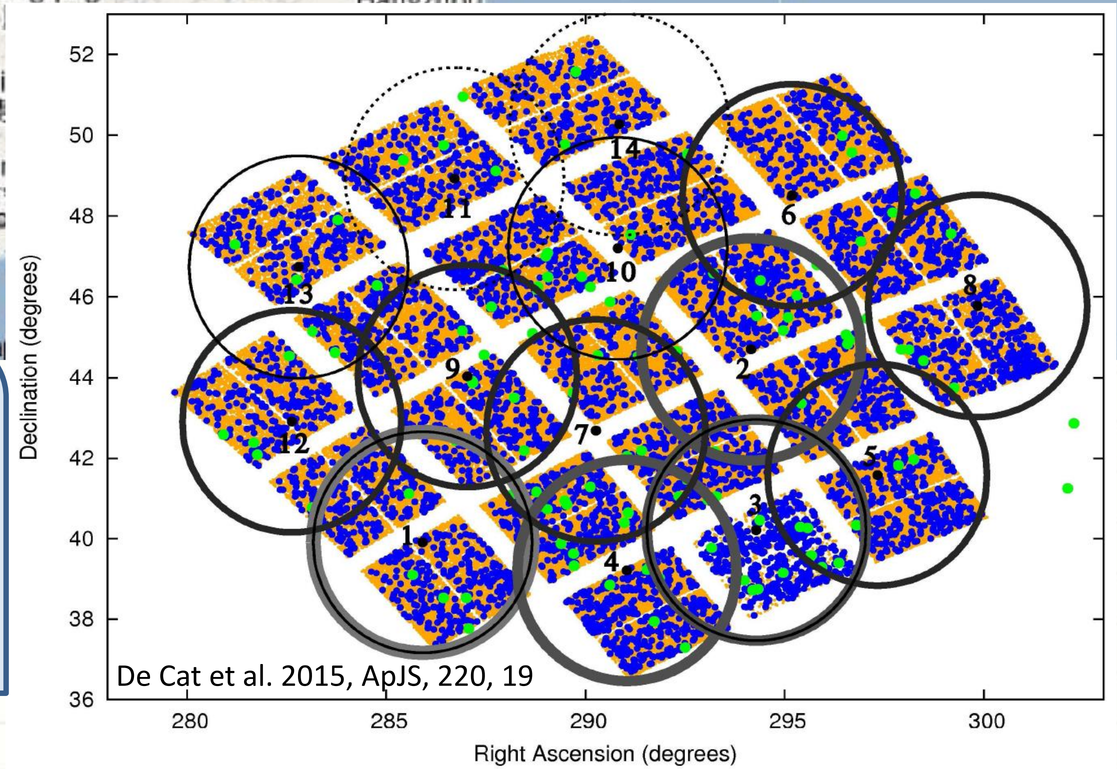

101,086 spectra acquired between 2011 and 2014
(KIC atmospheric parameters)

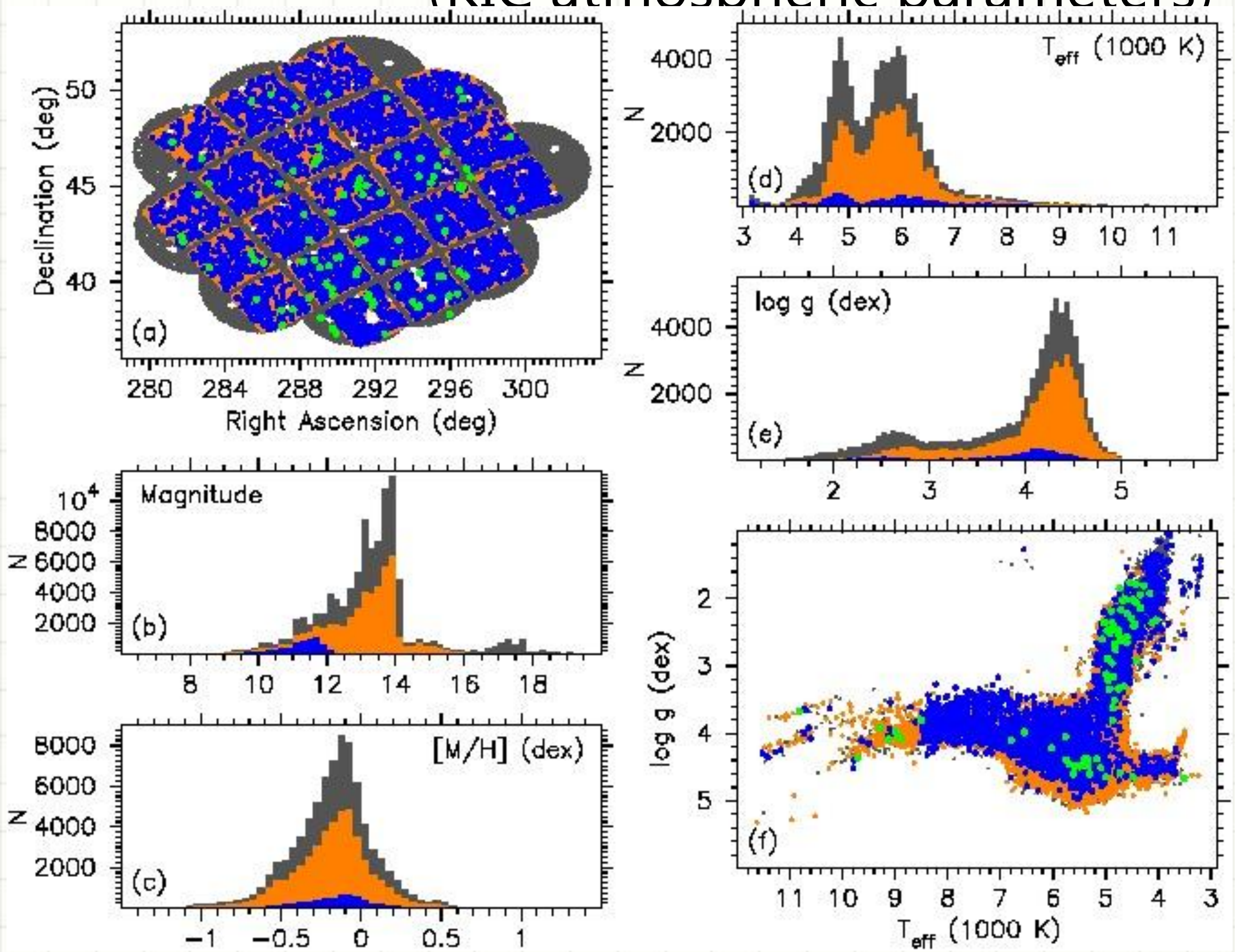

De Cat et al. 2015, ApJS, 220, 19

17,114 stars observed more than one time
(KIC atmospheric parameters)

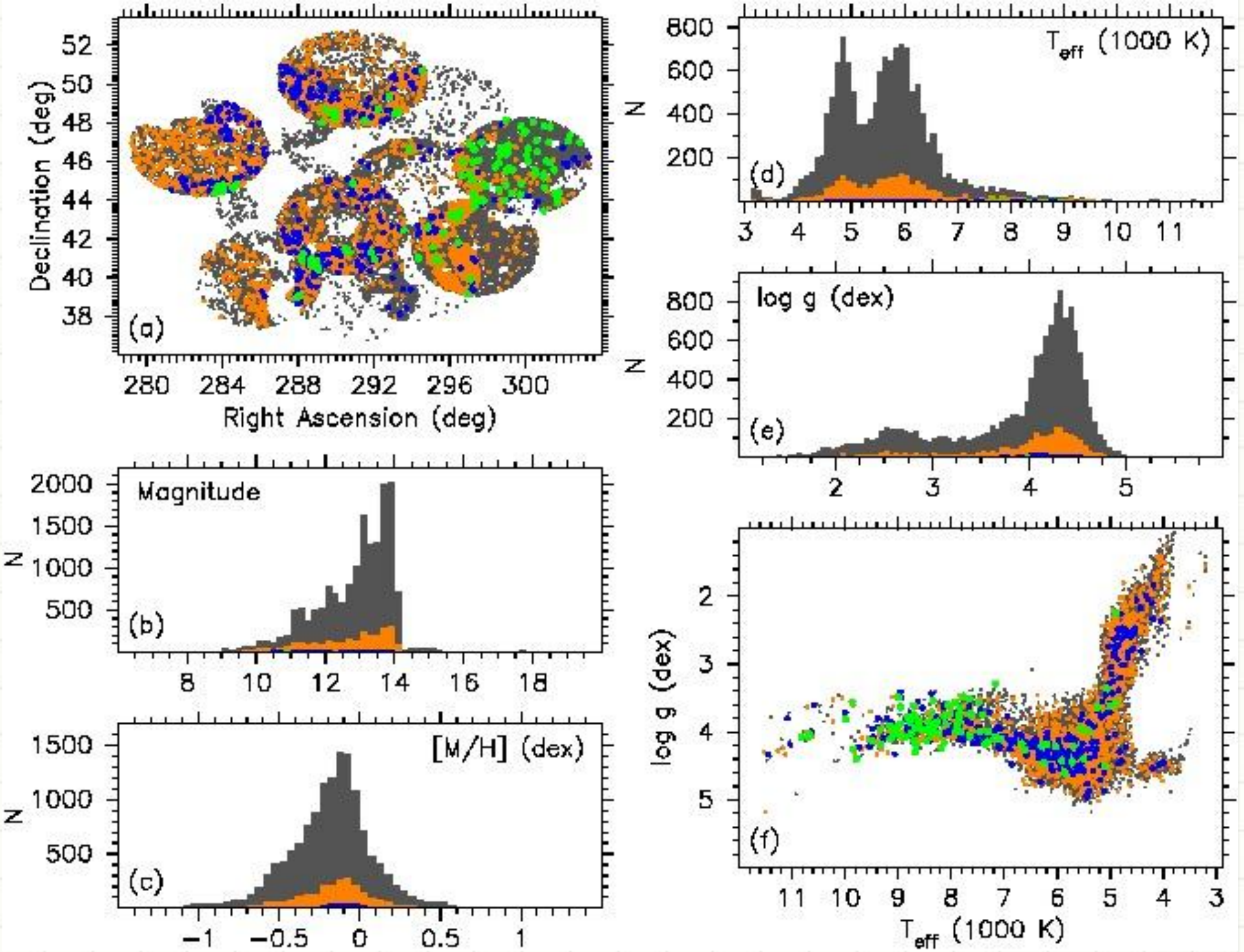

LAMOST spectra – examples

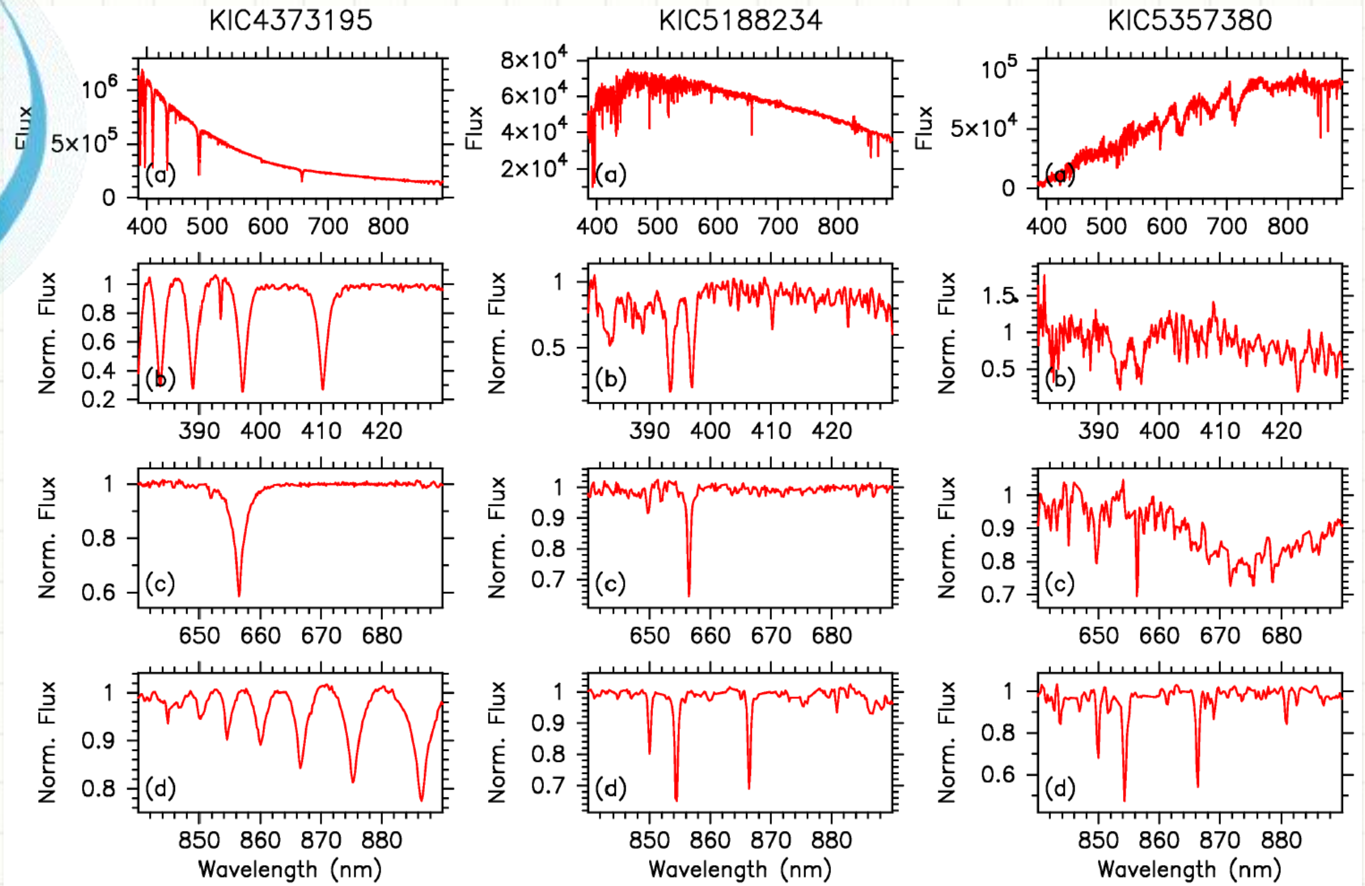

Examples of high-quality LAMOST spectra of A, F, and K-type stars: the full observed wavelength range (upper panels) and the continuum-normalized fluxes in three different wavelength regions: 380 − 430 nm, 640 − 690 nm, and 840−890 nm.

De Cat et al. 2015, ApJS, 220, 19

LAMOST spectra – signal-to-noise

Histograms of the signal-to-noise (S/N) ratio of spectra that were used to derive the atmospheric parameters (we derived the atmospheric parameters from 61,753 good quality spectra of **51,385** stars.)

The left and right panels show the S/N range [0,100] with bin size 10 and the S/N range [100, 600] with bin size 100, respectively.

The S/N was measured at the effective wavelengths of the Sloan DSS filters ugriz.

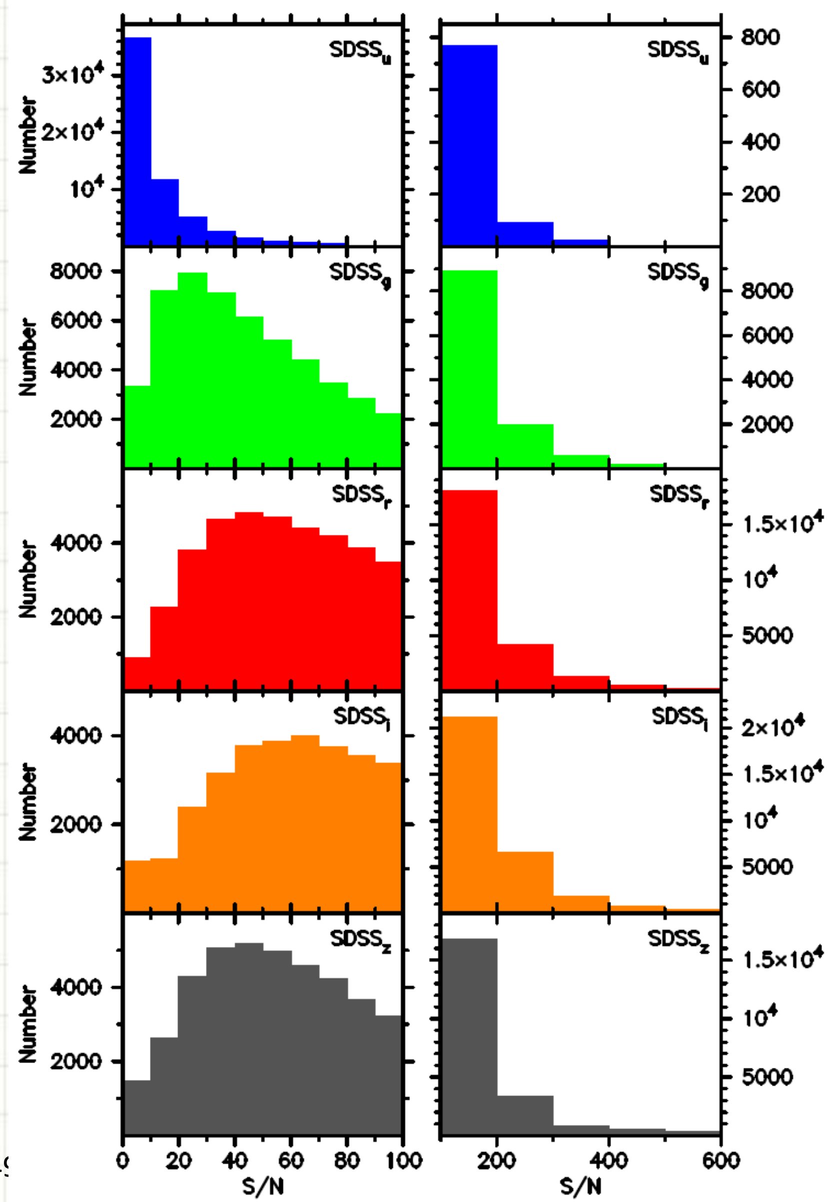

Frasca et al. 2016, A&A in press, arXiv: 16060914

ving the atmospheric parameters, RV, and vsini– examples

The code ROTFIT (Frasca et al. 2003, Frasca et al. 2006)

The continuum-normalized LAMOST spectra of an A, F, and K-type star in five spectral regions.

The best template found with ROTFIT is overplotted with a red line.

The difference between the two spectra is displayed at the bottom of each panel with a blue line.

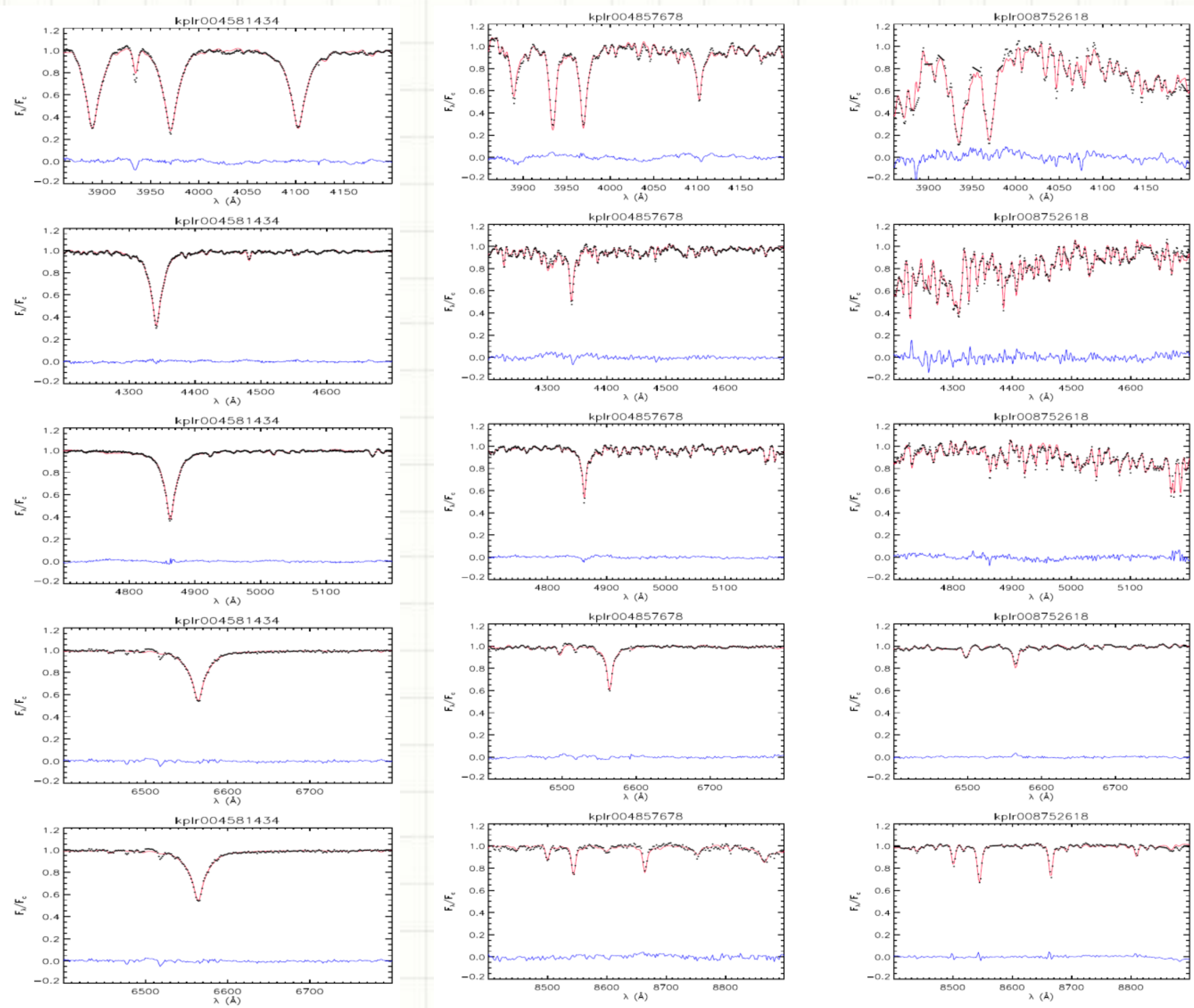

Frasca et al. 2016, A&A in press, arXiv: 160609149

Precision of the derived parameters

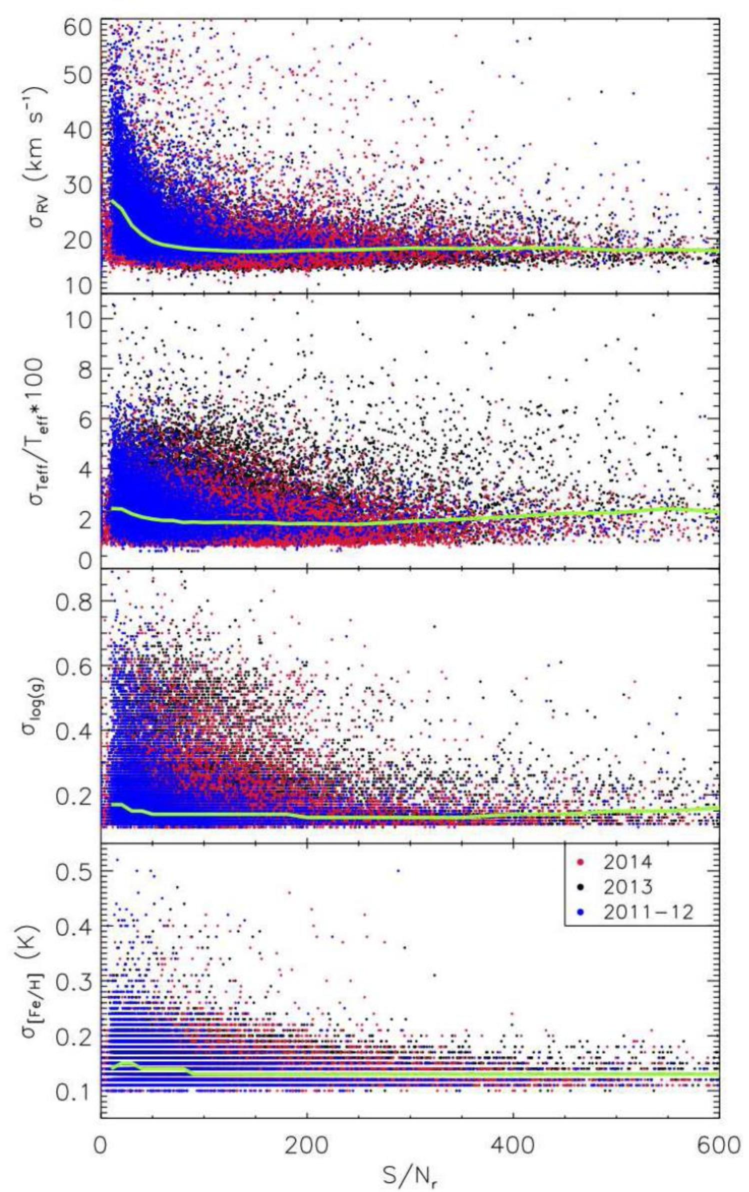

Scatter plots with the errors of RV, T_{eff}, log g, and [Fe/H] (from top to bottom) as a function of the S/N in the r band.

Blue dots: data from 2011-2012, black: data from 2013, and red: data from 2014.

The solid green line is the median value as a function of S/N.

Frasca et al. 2016, A&A in press, arXiv: 160609149

Accuracy of the derived parameters

Comparison between the RV measured on the LAMOST spectra with the literature values (mainly high resolution spectra). Dots: stars with multiple LAMOST observations.

The continuous line is the one-to-one relationship.

The differences, displayed at the bottom, show a mean value of ≃+5 km/s and a standard deviation of about 14 km/s.

Discrepant values are enclosed into squares in both panels.

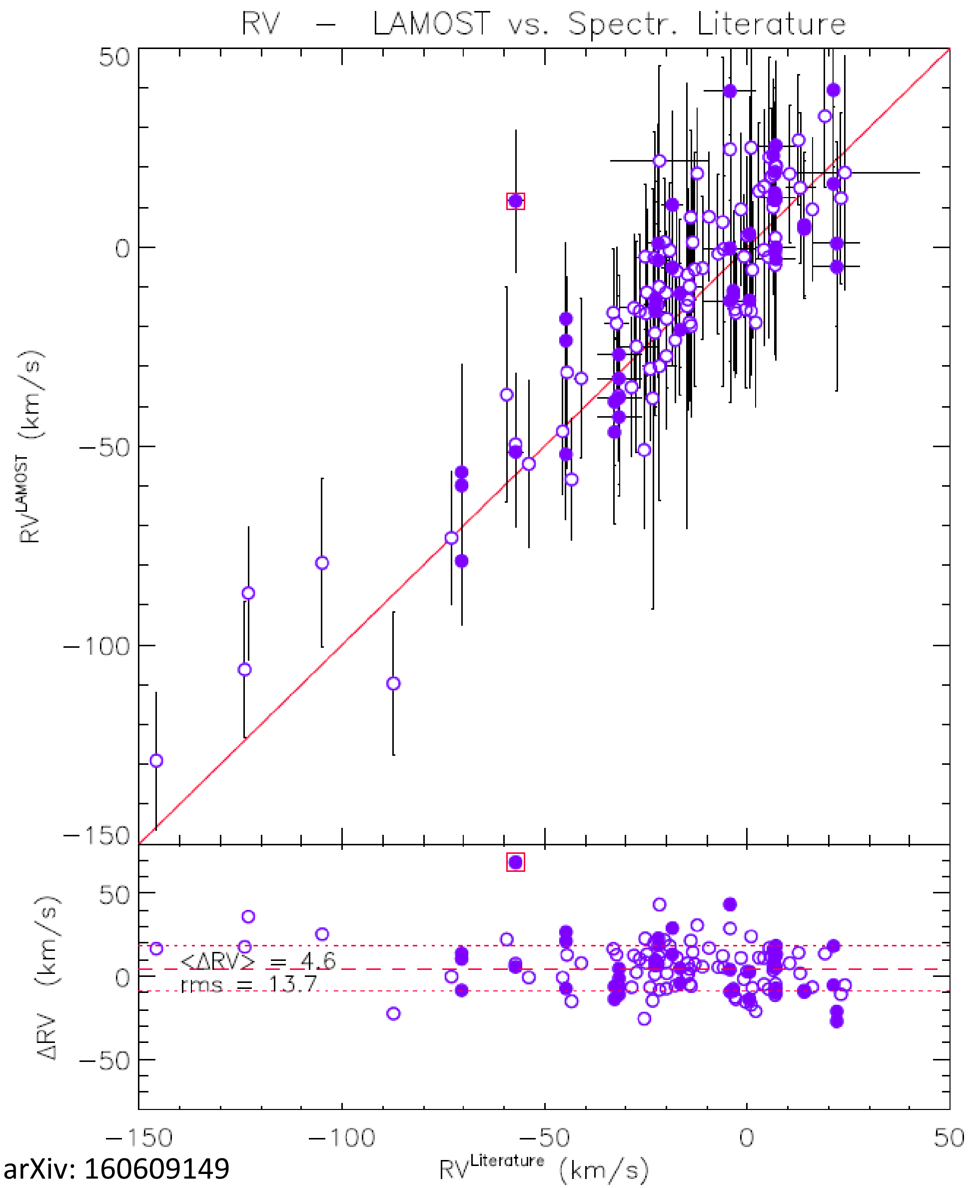

Frasca et al. 2016, A&A in press, arXiv: 160609149

Accuracy of the derived parameters

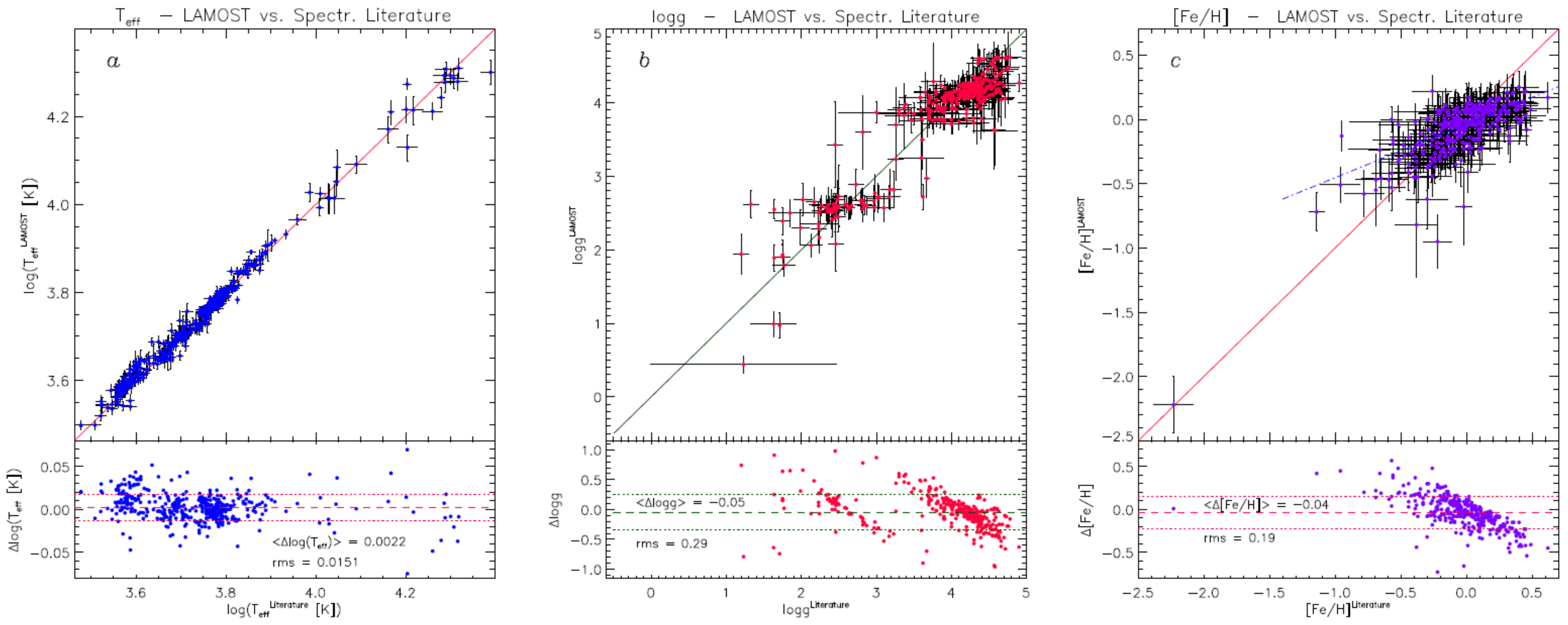

Frasca et al. 2016, A&A in press, arXiv: 160609149

Comparison between the atmospheric parameters measured on LAMOST spectra and the literature values. The dash-dotted line (panel c) is a linear fit to the data with $[Fe/H]_{Lit} > -1.5$.

Accuracy of the derived parameters

log *g* derived with ROTFIT *v.s.* the values the literature (blue dots), the APOKASC (red dots), and the SAGA (green asterisks) catalogues.

Linear fits to the data with log *g* <3.3 and log *g* ≥ 3.3 are displayed by the dash-dotted and the dashed lines, respectively.

The open diamonds in the bottom panel refer to values corrected according to equations:

$$\log g_{\rm corr} = 2.01 \cdot \log g - 2.70 \qquad (\log g < 3.3)$$
$$\log g_{\rm corr} = 1.88 \cdot \log g - 3.55 \qquad (\log g \geq 3.3)$$

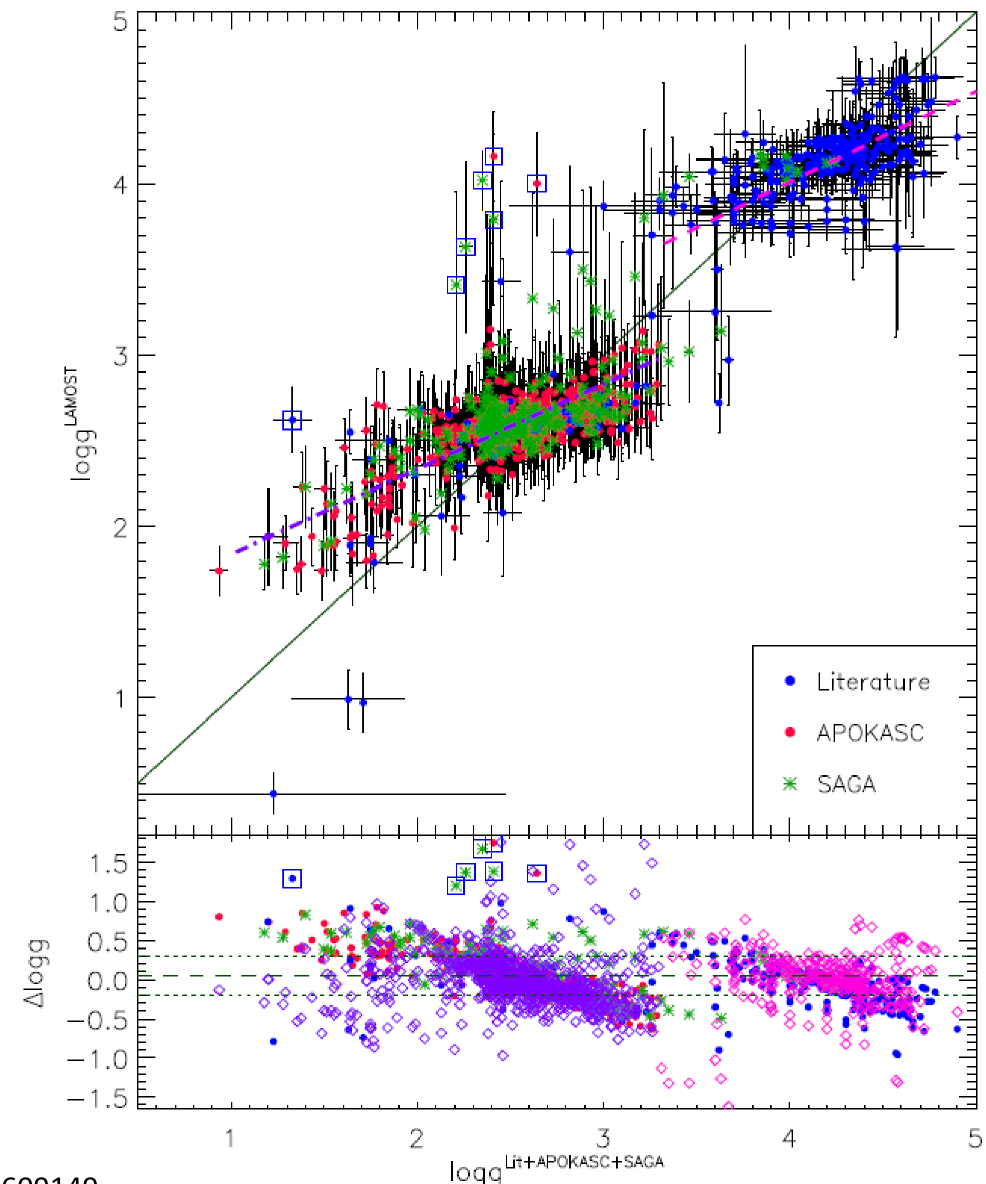

Frasca et al. 2016, A&A in press, arXiv: 160609149

Accuracy of the derived parameters

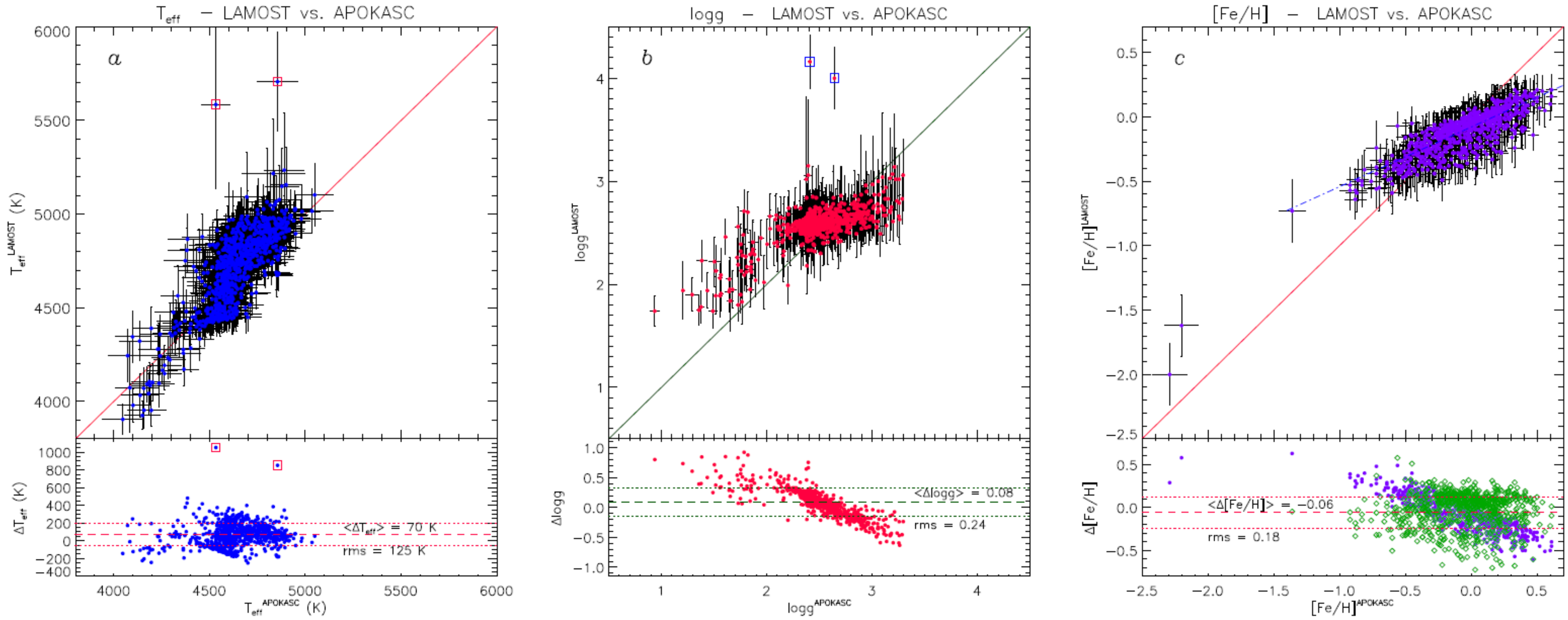

Frasca et al. 2016, A&A in press, arXiv: 160609149

Comparison between the atmospheric parameters measured on LAMOST spectra and the red giants in the APOKASC catalog (Pinsonneault et al., 2014, ApJS 215, 19). The linear fit to [Fe/H]>-1.0 LAMOST values:

$$[\mathrm{Fe/H}]_{\mathrm{corr}} = 2.16 \cdot [\mathrm{Fe/H}] + 0.17$$

Accuracy of the derived parameters

Comparison between the corrected [Fe/H] with those from the KIC and Huber et al. (2014).

30,104 stars in common between these catalogues.

Pinsonneault et al. (2012) *"A Revised Effective Temperature Scale for the Kepler Input Catalog"* – T_{eff} defined at a fixed [Fe/H] = −0.2

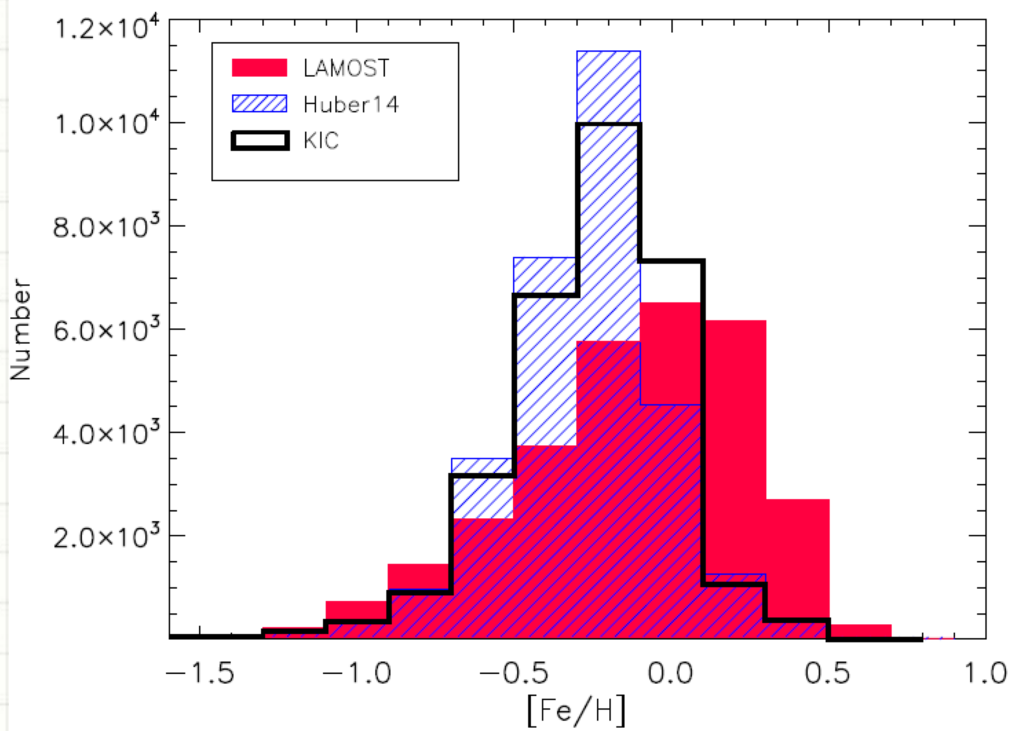

	Mean	Median
LAMOST	-0.05	+0.02
KIC	-0.17	-0.13
Huber (all stars in common)	-0.19	-0.16
Huber (spectroscopic values)	-0.02	-0.01

Frasca et al. 2016, A&A in press, arXiv: 160609149

Spectral peculiarities and chromospheric activity in the LAMOST spectra

Peculiarities in the LAMOST spectra (e.g. barium stars or λ Boo stars) can be detected – see poster A2 by Corbally et al. and the paper by Gray et al. (2016, AJ 151, 13)

Emission lines – magnetic activity in late-type stars or the circumstellar environment and winds in hot stars.

Ca II H & K lines (diagnostics of the chromospheres) lie in the spectral region where the LAMOST efficiency is low. The flux emitted by cool stars in that region is very low → with the exception of the brightest targets, Ca II H & K lines are dominated by noise.

Detection of active stars

Balmer Hα line to identify late-type or early-type stars with emission that can be produced by various physical mechanisms.

Subtract from each LAMOST spectrum the Indo-US template that best matches the final APs.

Integrate the residual Hα emission, $EW^{res}_{H\alpha}$, over a wavelength interval of 35 Å around the line center and select stars with $EW^{res}_{H\alpha} \geq 1$Å as emission-line candidates.

Spectra with T_{eff} < 5000K and a log g > 3.0 (K and M dwarfs): integrate the residual Hα profile over the range of 16 Å and adopt $EW^{res}_{H\alpha}$ > 0.3 Å for keeping a star as a candidate.

Inspect the selected spectra visually and reject false positives (mismatch in the line wings between target and template, cosmic ray spikes, spectra with a very low signal).

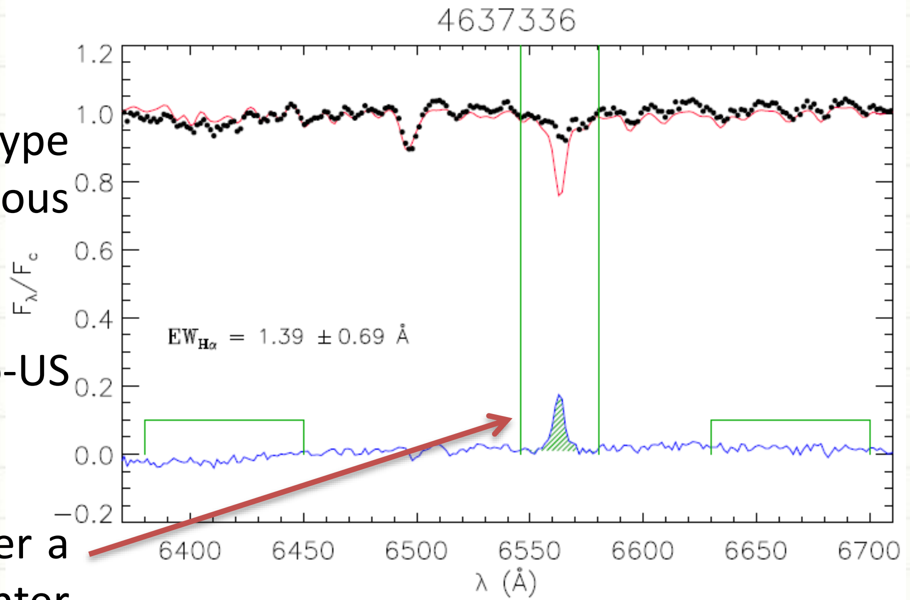

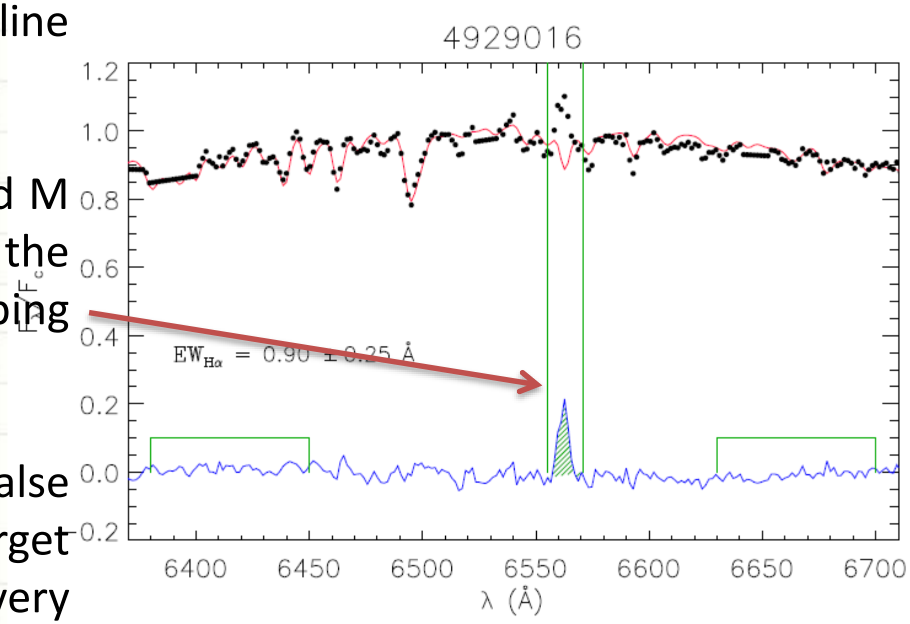

Frasca et al. 2016, A&A in press, arXiv: 160609149

Unexpected nebular lines

Emission lines at the two sides of the Hα emission that are the forbidden lines of [N II] at λ 6548 and λ 6584 Å.

These emission features can be a result of nebular emission that has not been fully removed by the sky subtraction.

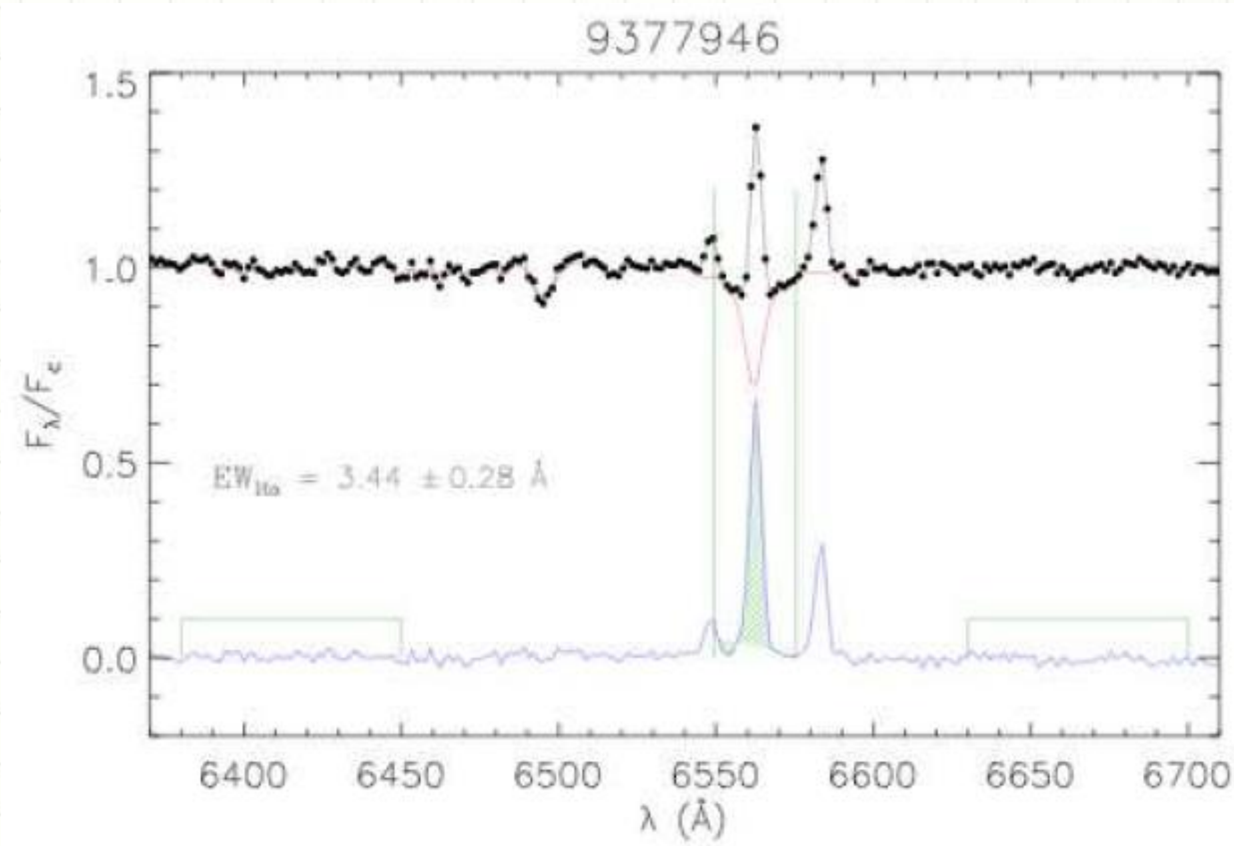

Frasca et al. 2016, A&A in press, arXiv: 160609149

Detection of chromospherically active stars

547 stars (577 spectra) display Hα in mission or filling in by the minimum amount defined above.

For these stars, we investigated the behaviour of the Ca II IRT lines (for late-type active stars, the emission which fills the cores of the Ca II lines originates from a chromosphere.)

Analysis: we subtracted the same non-active template that was used for Hα, and measured the values of EW^{res}_{8498}, EW^{res}_{8542}, and EW^{res}_{8662} .

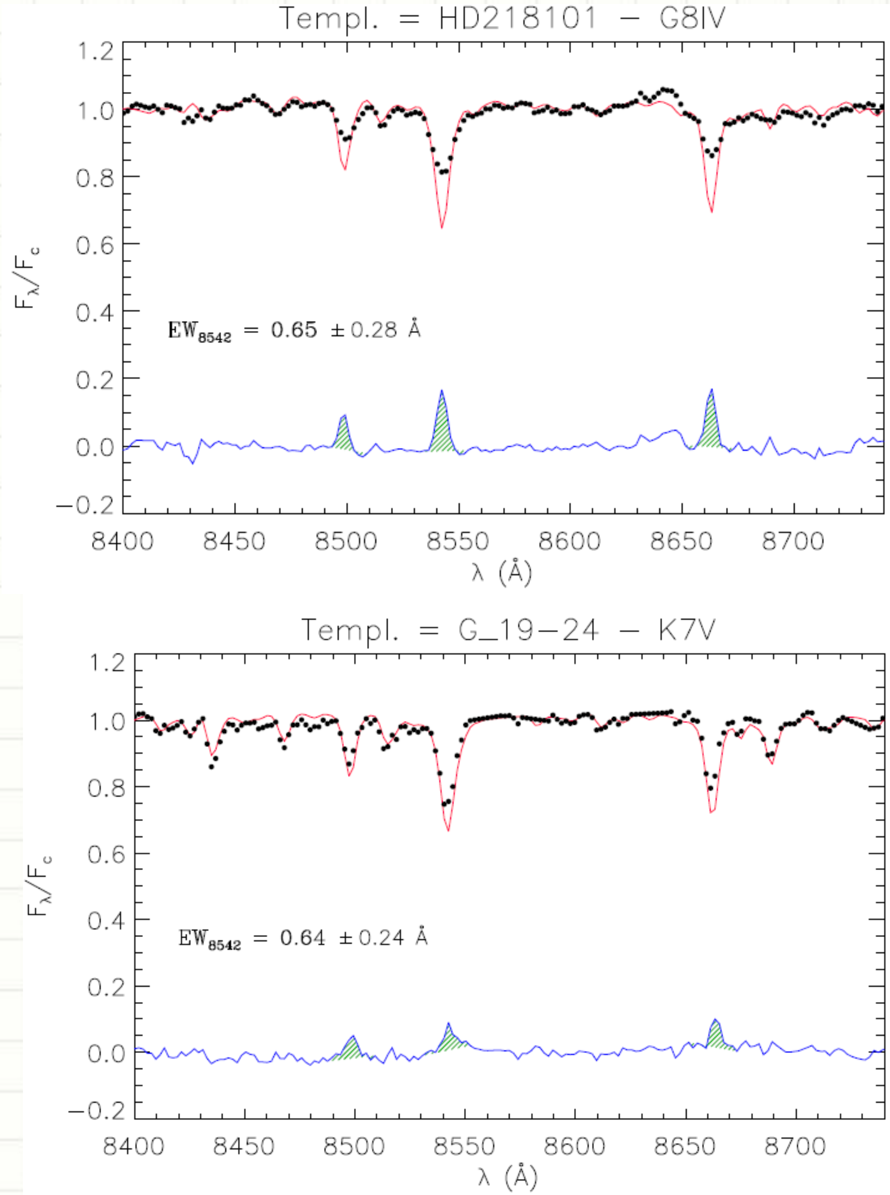

Frasca et al. 2016, A&A in press, arXiv: 160609149

Indicators of chromospheric activity: *F* and *R'*

- The **surface line flux**, *F*
- The **ratio between the line luminosity and the bolometric luminosity**, *R'*
  - **Hα**: $F_{H\alpha} = F_{6563} EW^{res}{}_{H\alpha}$
    - F_{6563} is the continuum surface flux at the Hα center evaluated from the NextGen synthetic low resolution spectra (Hauschildt et al. 1999) at the stellar temperature and surface gravity of the target.
    - $R'_{H\alpha} = L_{H\alpha}/L_{bol} = F_{H\alpha}/(\sigma T^4{}_{eff})$.
  - **Ca II IRT**: The line fluxes in the three Ca II IRT lines have been calculated with similar relations, where the continuum flux at the center of each line has been also evaluated from the NextGen spectra.

Hα flux and $R'_{H\alpha}$ versus T_{eff}

Dashed line: boundary between chromospheric emission (below it) and accretion as derived by Frasca et al. (2015).

Green asterisks: questionable emission

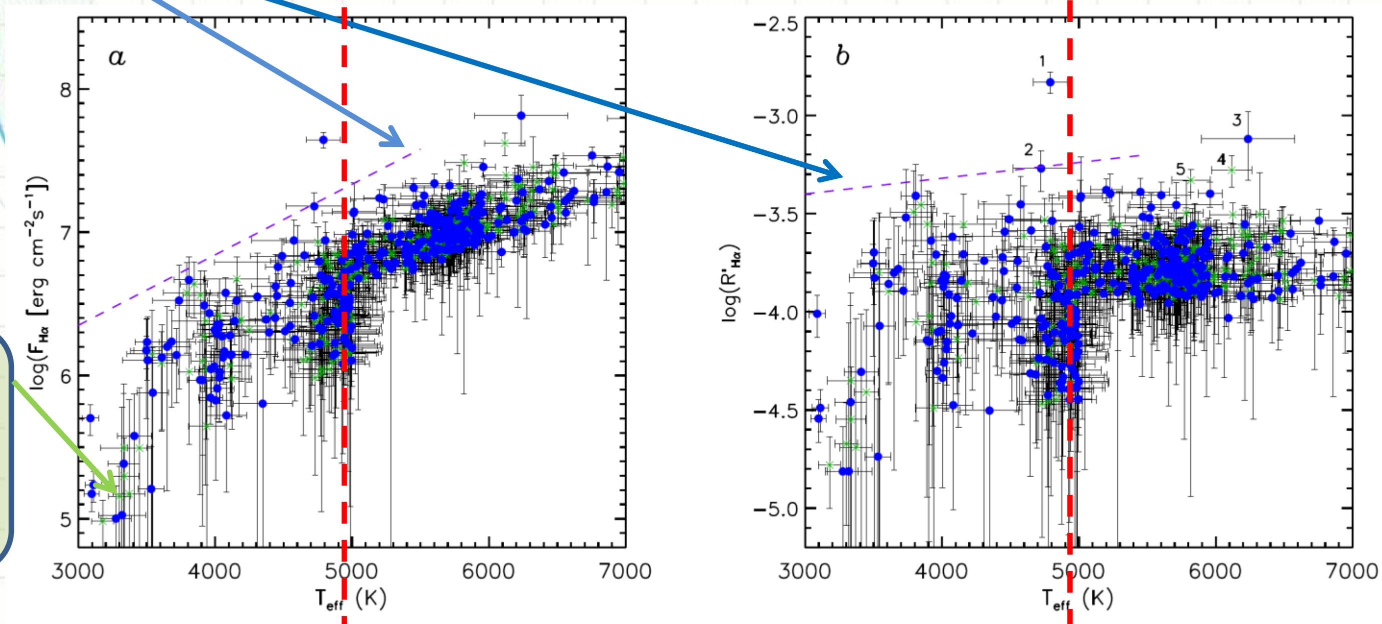

Frasca et al. 2016, A&A in press, arXiv: 160609149

Different lower level of fluxes and R' for stars with T_{eff} < 5000 K and T_{eff} > 5000 K is the result of different thresholds adopted for selecting active stars in these two T_{eff} domains.

Hα flux and $R'_{\mathrm{H}\alpha}$ versus T_{eff}

KIC 8749284 (K1 V) – the only star in the domain of accerting objects.

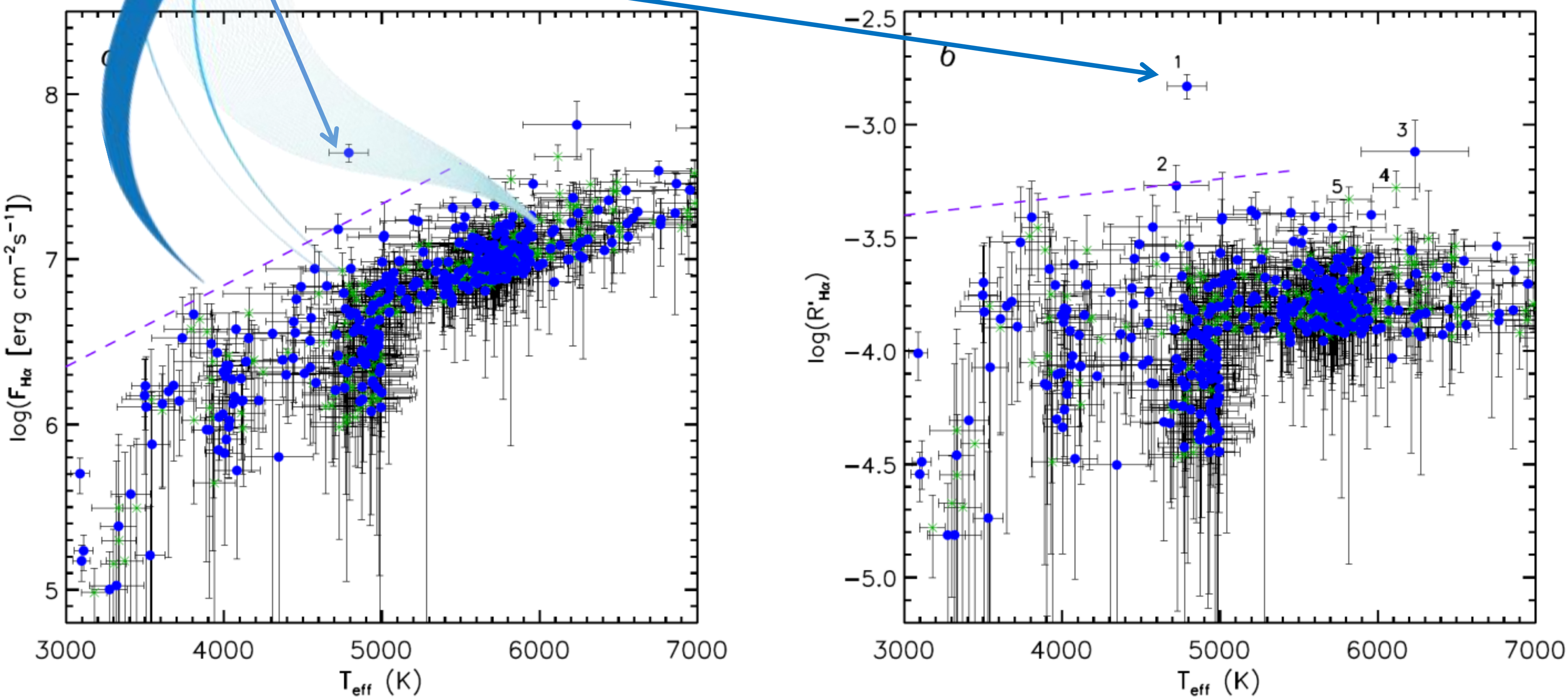

Frasca et al. 2016, A&A in press, arXiv: 160609149

Young accreting star KIC 8749284

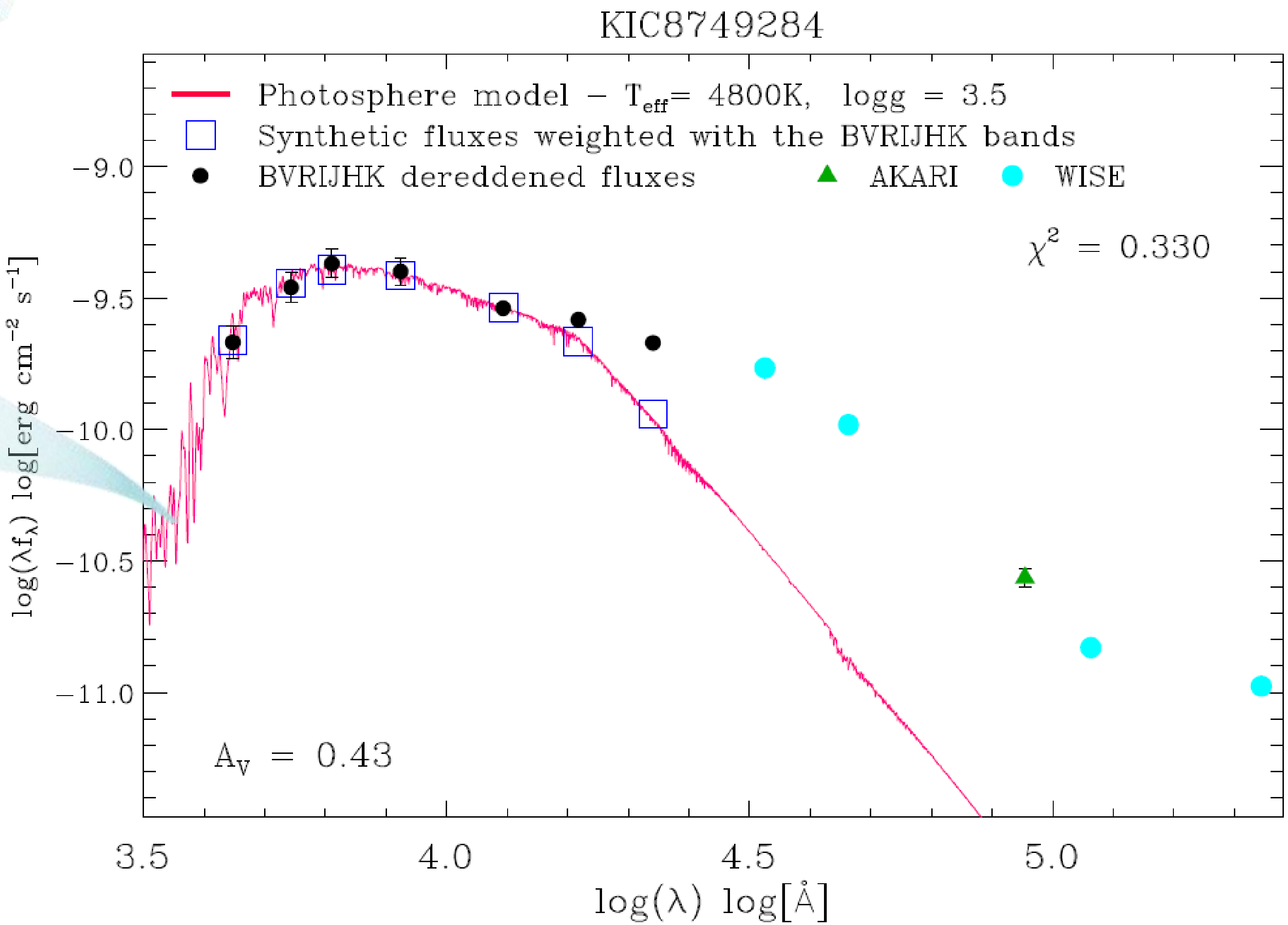

Frasca et al. 2016, A&A in press, arXiv: 160609149

The spectral energy distribution (SED) clearly shows an IR excess starting from the *H* band, which is compatible with an ‘evolved’ circumstellar disk of a Class II source (pre-main-sequence stars with optically thick disks).

Hα flux and $R'_{H\alpha}$ versus T_{eff}

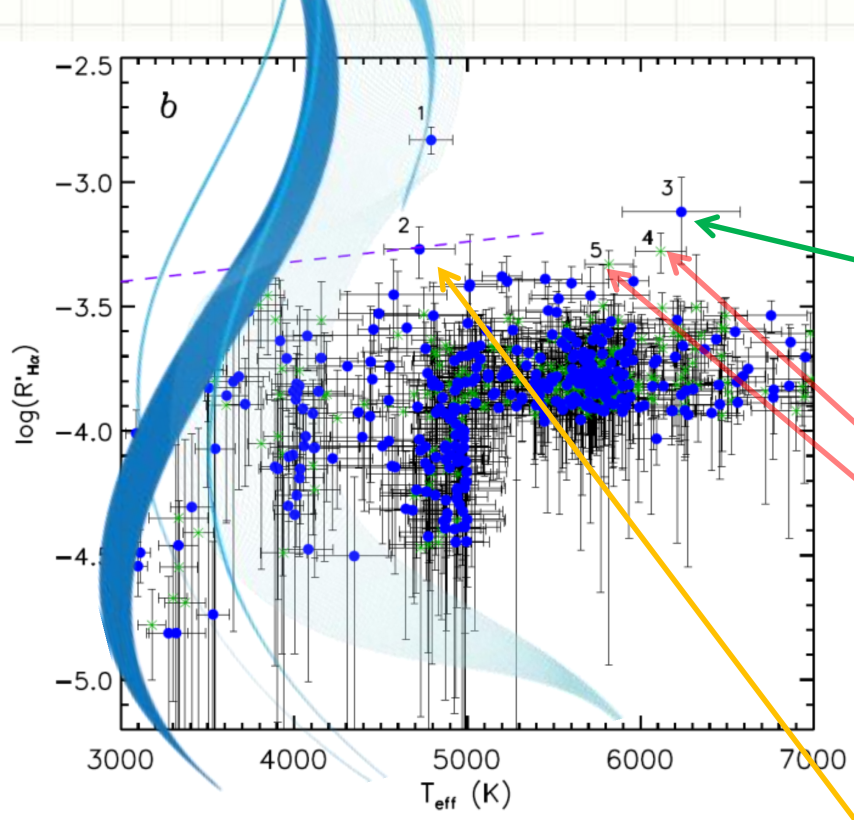

KIC 4644922 is a candidate post-AGB star surrounded by a dusty disk for which the Hα emission originates in the circumstellar environment (Gorlova et al. 2012).

KIC 8722673 and KIC 9377946 display nebular emission at the two sides of Hα → strong Hα flux may not be of chromospheric origin but it may be a result of sky line emission which overlaps the stellar spectrum.

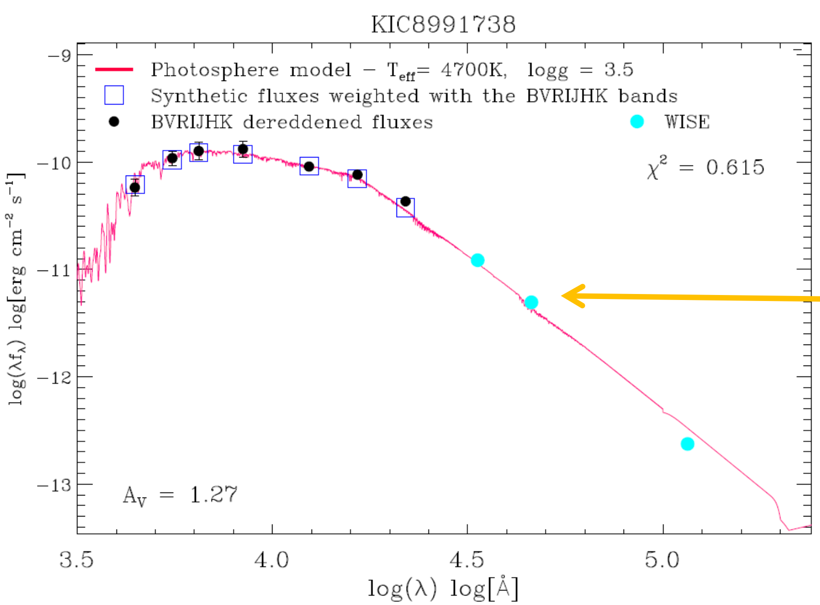

KIC 8991738 – no IR excess in SED, no Kepler data

Frasca et al. 2016, A&A in press, arXiv: 160609149

Flux–flux relationship between Hα and Ca II IRT

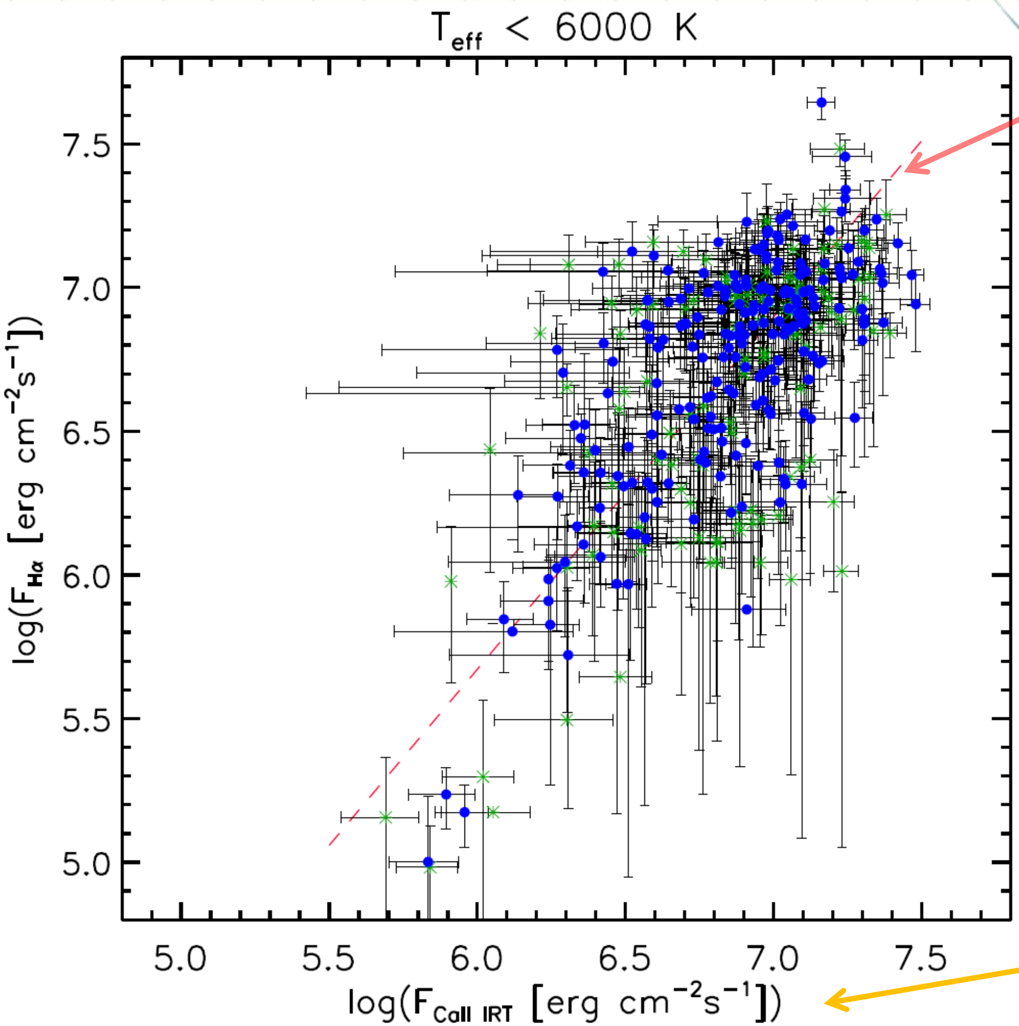

The least squares regression yields the relation: $\log F_{H\alpha} = -1.85 + 1.25 \cdot \log F_{\text{CaII IRT}}$

That power-law with an exponent larger than 1 for the flux–flux relationship is in agreement with previous results.

442 GKM stars which we classify as chromospherically active.

$F_{\text{CaII IRT}}$ is the sum of the flux in each line of the triplet.

Frasca et al. 2016, A&A in press, arXiv: 160609149

The Hα and Ca II IRT flux versus P_{rot}

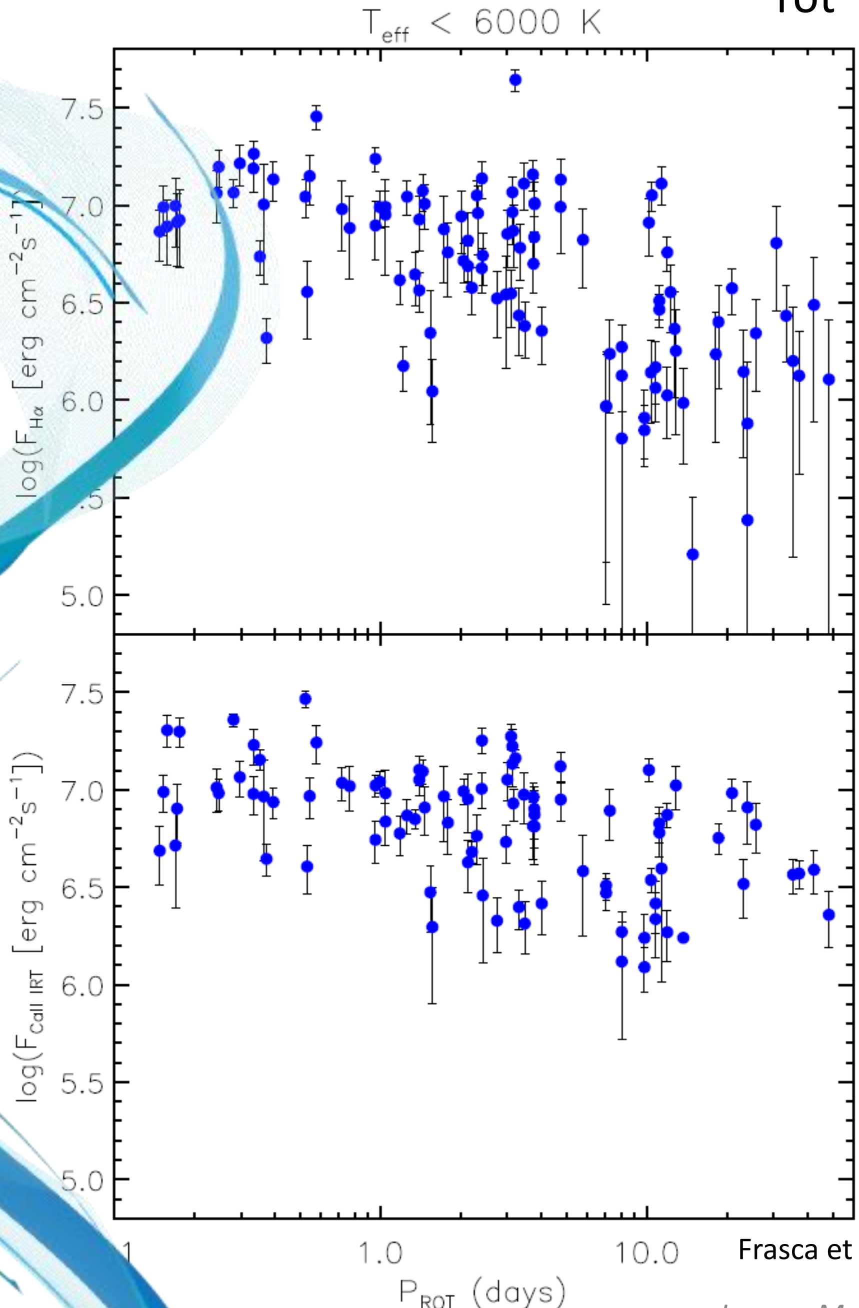

Rotation periods from the literature for about 200 stars.

As expected, we found that Hα flux increases with decreasing rotation period.

The low resolution of the spectra, which gives rise to rather large flux errors, and the heterogeneous sample which includes stars with very different properties are the main responsible for the large data scatter.

All those results have been summarized in table A.4 by Frasca et al. (2016).

Frasca et al. 2016, A&A in press, arXiv: 160609149

Future of the LAMOST-Kepler project

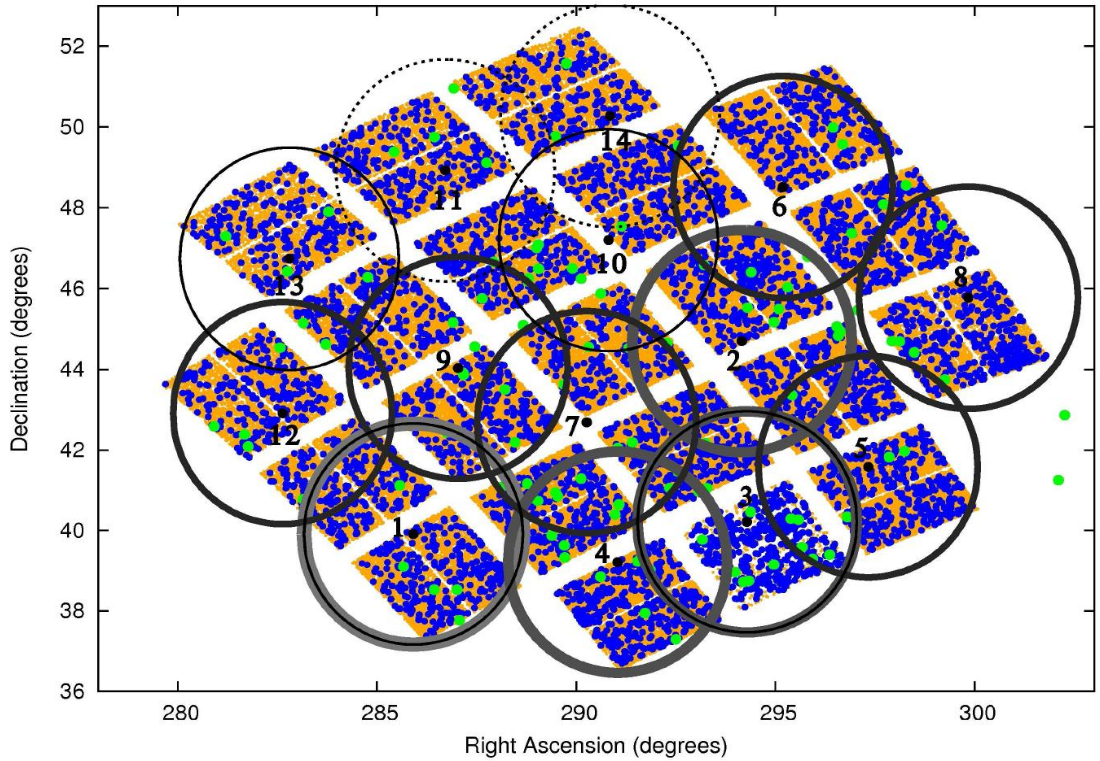

2015 and 2016: observations of those stars for which we did not obtain useful data in the first round of the Project.

Future of the LAMOST-Kepler project – K2 fields?

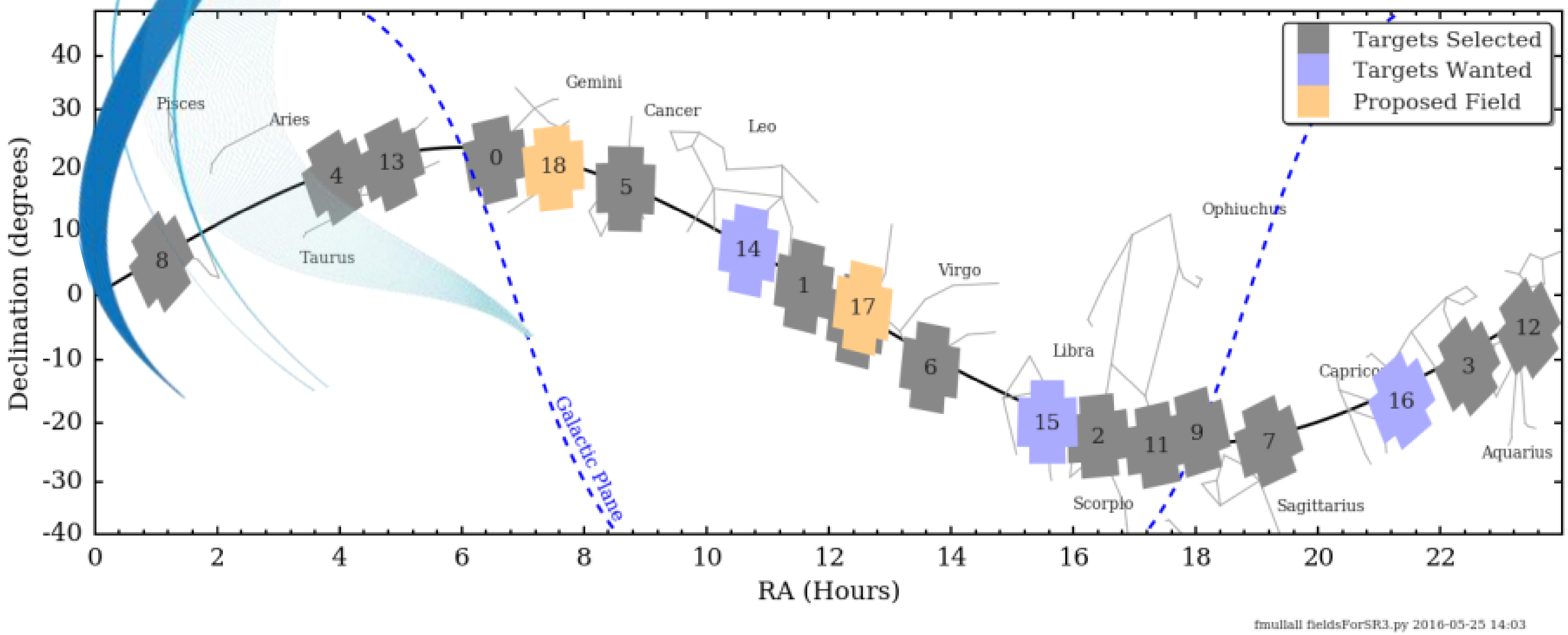

Are we going to observe the K2 fields for the next 100 years?

How about 20?

2nd LAMOST-Kepler workshop

When	**Most probably the last week of July 2017**
Where	Brussels, Belgium
Why	Discussion of the scientific aims, observing strategy, target selection, methods of data reduction and analysis, and all other issues which can help us make the full use of the opportunities offered by the LAMOST instrument.